Catadioptric Camera Calibration using Planar Calibration Objects

A thesis presented

by

Cheng-I Chen

to

Institute of Computer Science and Engineering

College of Computer Science

in partial fulfillment of the requirements

for the degree of

Master

in the subject of

Computer Science

National Chiao Tung University

Hsinchu, Taiwan

2006

Catadioptric Camera Calibration using Planar Calibration Objects

by

Cheng-I Chen

Abstract

Catadioptric camera has been widely used in the applications of video surveillance and robot navigation due to its advantage of large field of view. However, it is more difficult to calibrate this kind of cameras than to calibrate perspective cameras because the camera structure is more complicated and there are more camera parameters to be determined. Catadioptric camera can be either central or non-central, depending on whether it keeps the single viewpoint constraint. The central catadioptric camera has a single center of projection, hence the epipolar geometry can be applied to calibrate the camera parameters. Considering the practical issues, such as the large size of central catadioptric camera and the difficulty of precise alignment between the camera and the mirror, most off-the-shelf catadioptric cameras are non-central ones without obeying the single viewpoint constraint. A non-central catadioptric camera can be calibrated by photogrammetric methods requiring the correspondence of 3-D world coordinate and 2-D image coordinate.

In this thesis, we propose novel calibration methods for determining camera parameters of both central and non-central catadioptric cameras. Our methods utilize planar objects and can achieve very accurate results while keeping the calibration procedures simple. For central catadioptric camera, 2-D projection point in image for a 3-D projection ray can be determined by the viewing sphere model. In the proposed calibration procedure, we place a planar calibration plate several times surrounding the camera and capture an image for each pose of the calibration plate. With the viewing sphere model and the associated parameters, we can unwarp the captured catadioptric image into the image captured by a virtual perspective camera with known intrinsic parameters as well as extrinsic parameters relative to the viewing sphere. We show that moving a calibration plate around the catadioptric camera is equivalent to placing the same calibration plate at different poses relative to a static, virtual, perspective camera. We can then use this set of unwarped perspective images to calculate the relative poses of the calibration plate as well as the projection error of the feature points on the calibration plate by using the homography method. The associated parameters of the viewing sphere model can be obtained by minimizing the projection error in a nonlinear optimization procedure.

For non-central catadioptric camera, the single viewpoint constraint does not hold and

the viewing sphere model cannot be applied. Thus it is even more difficult to calibrate a non-central catadioptric camera. In this work we determine the projection model of the non-central catadioptric camera through a calibrated central catadioptric camera as an intermediate. First, we use a set of LCD panels with fixed positions to present feature patterns to the central catadioptric camera. Image coordinates of these feature patterns in the captured images are automatically determined and the corresponding 3-D coordinates can be calculated since the camera is calibrated. The same set of LCD panels are then presented to the non-central catadioptric camera. For each feature point, we can obtain its 2-D coordinate in the image captured by the non-central catadioptric camera. Since the 3-D coordinates of the feature points are determined beforehand, camera parameters of the non-central catadioptric camera can then be obtained photogrammetrically. In the proposed method, we use Mashita's method to determine the initial values of the parameters in the reflected ray model and then optimize the values of the parameters by minimizing the projection error.

Experiments with simulation and real data clearly demonstrate the robustness and accuracy of the proposed calibration methods. In the simulation data, we add gaussian noise with zero-mean and standard deviation ($\sigma = 0.0 \sim 2.0$) to evaluate the performance of proposed methods. The results show that our methods are indeed robust and accurate. We also implement calibration method using geometric invariants for the purpose of comparison. The results show that our methods are indeed robust and accuracy, and have better performance than one using geometric invariants. Moreover, we also present an integrated surveillance system in which the calibrated non-central catadioptric camera is used to navigate a mobile robot for patrolling.

Contents

List of Figures

List of Tables

Chapter 1

Introduction

Figure 1.1: **The phenomenon of pinhole photography.**
Graph source : http://brightbytes.com/cosite/tradecards.html

1.1 Background

1.1.1 History of the Camera

"Eyes are the window to the soul."

Because of the eyes, human beings can see the flowers, green grass, blue sky and this beautiful world. Eyes make people can see each other, communicate to each other and moreover make our life colorful.

For the purpose of visualizing the vision what we see, scientists invented series imaging devices. The fundamental of the camera is **pinhole photography** (figure 1.1). Go into a very dark room on a bright day. Make a small hole on the wall and look at the opposite wall. Then we will see the world outside the window upside down. This phenomenon can be explained by a simple law of the physical world. Light travels in a straight line and when some of the rays reflected from a bright subject pass through a small hole in thin material, they do not scatter but cross and reform as an upside down image on a flat surface held parallel to the hole.

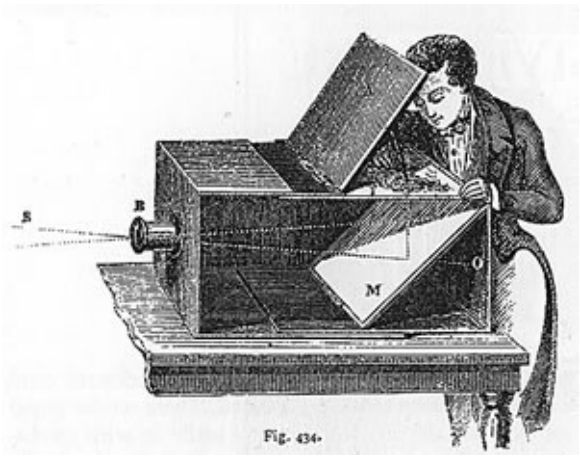

Figure 1.2: **Camera obscura.** Graph source : http://facultyweb.anderson.edu/ krrudynski/

In 5th century, the Chinese philosopher *Mo-Ti* first describe the phenomenon in Mo-Ching. He formally recorded the creation of an inverted image formed by light rays passing through a pinhole into a darkened room. He called this darkened room a ”collecting place” or the ”locked treasure room.” In 1797, the famous artist, *Leonardo da Vinci*, also gave clear descriptions of the phenomenon in his notebooks. The description is as following.

”Who would believe that so small a space could contain the image of all the universe? O mighty process! What talent can avail to penetrate a nature such as these? What tongue will it be that can unfold so great a wonder? Verily, none! This it is that guides the human discourse to the considering of divine things. Here the figures, here the colors, here all the images of every part of the universe are contracted to a point. O what a point is so marvelous!”

Until early 17th century, the term **”camera obscura”** (figure 1.2) was first used by the German astronomer *Johannes Kepler*. Camera obscura means **”dark room”** in Latin and is the predecessor of camera. In 17th and 18th century, artists use camera obscura to help them draw landscapes, buildings and portraits. The structure of the camera obscura is like single-lens reflex (SLR) camera in use today. Light rays that travel into the wooden box through the lenses are reflected by a planar mirror. A real image will be imaged on a ground glass, thus artists can sketch the contour of the image to draw pictures more realistically by a camera obscura.

(a) The first camera in the world (b) Image of the camera

Figure 1.3: **The first camera in the world and its image.**
Graph source : http://inventors.about.com/library/inventors/bldaguerreotype.htm

In 1839, the first camera has been invented, surprisingly, by a French artist, *Louis Jacques Mande Daguerre* (figure 1.3). The most important of this work is the invention of the **imaging sensor**. The imaging sensor he invented is a silver-plated copper plate. The silver-plated copper plate had first to be cleaned and polished until the surface looked like a mirror. Next, the plate was sensitized in a closed box over iodine until it took on a yellow-rose appearance. The plate, held in a lightproof holder, was then transferred to the camera. After exposure to light, the plate was developed over hot mercury until an image appeared. Although the imaging process is very complicate and inefficient, we do not have to draw the picture by ourselves. Then, the history of the camera begins.

After the evolution of almost two centuries , the technology of cameras is improved significantly. The color of the image is from monochrome to autochrome. The resolution of the image is also much higher than before. The size of the camera is from the wooden box to a button. The imaging sensor is from the silver-plated copper plate to the films, and to the charge coupled device (CCD), complementary metal oxide semiconductor (CMOS) and X3. The evolution will keep going in every respect of camera. Cameras with more colorful image, higher resolution, smaller size and better user interface will be invented in the future (figure 1.4).

(a) Modern digital camera (b) Image of modern camera

Figure 1.4: **Modern camera and its image.**

1.1.2 Omnidirectional Vision

Although the quality of cameras are getting better and better, the field of view of conventional cameras are still very small. Since the size of imaging device (CCD array, for instance) is finite size and the camera lens occludes itself while receiving incoming rays, the lens typically has a small field of view that corresponds to a small cone rather than a hemisphere. Because of the limited field of view, conventional cameras are restricted in a variety of vision applications.

The supreme goal of enlarging field of view is the **omnidirectional vision** (figure 1.5) [37]. A omnidirectional camera can, at any instant in time, "see" in all directions. Such an omnidirectional camera would have an impact on a variety of applications, including robot navigation, surveillance, video conference, and scene reconstruction.

It is very important to describe that why every camera should have a **single projection center**. Notice the omnidirectional camera in figure 1.5. The light rays all radiated from a single projection center. The single viewpoint permits the construction of pure perspective images from the omnidirectional image. In the chapter 3, we will describe the process of the construction in detail. Any image computed in this manner preserves linear perspective geometry because of the single viewpoint. Besides, we can construct a panoramic image

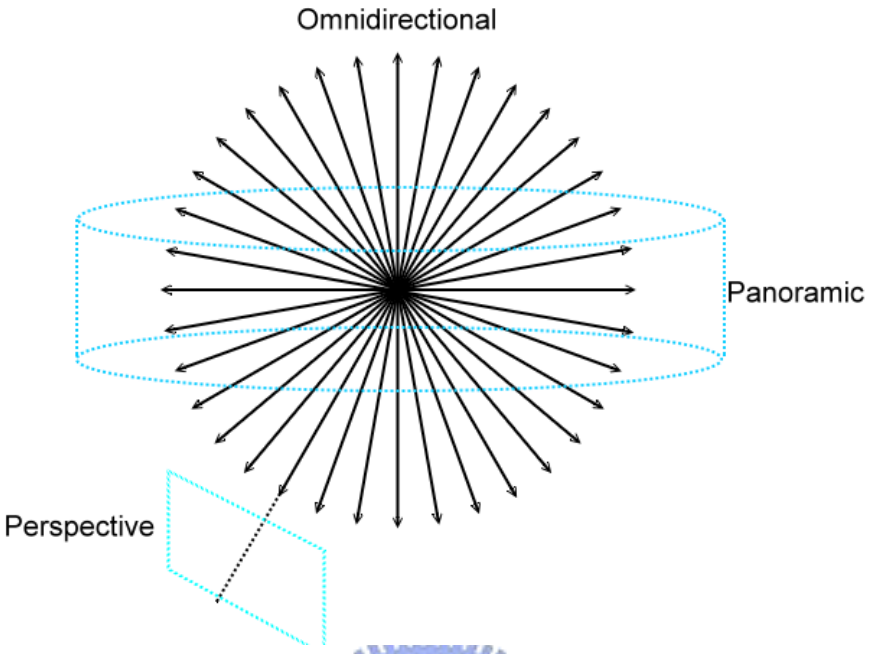

Figure 1.5: **Omnidirectional imaging sensor.**

using cylindrical projection, and the linear perspective geometry is also preserved in this case.

To achieve the goal of omnidirectional camera, many scientists and investigators developed many imaging devices to enlarge the field of view. The methods can be classified into three major categories, **rotating imaging systems** [1, 8, 10, 46], **fish-eye lenses** [12, 20]and **catadioptric systems** [7, 21, 28, 33, 49]. Here is a brief review of the three methods.

Rotating Imaging Systems The first solution is to rotate the entire imaging system about its center of projection (figure 1.6 (b)). The sequence of images acquired by rotation are ”stitched” together to obtain a panoramic view of the scene. The advantage of the method is large image resolution, because the panoramic image is composed by many real perspective images. Such an approach has been recently proposed by several investigators, and the most novel one is the systems developed by Ahuja which uses a camera with a non-frontal image detector to scan the world.

The first disadvantage of these methods is that the rotation mechanism have to move very precisely to keep the single viewpoint constraint. It also needs much time to take a sequence of images. After capturing images, we need to stich them together. This drawback restricts the use of rotating systems to static scenes and non-real-time applications.

Fish-Eye Lenses Another solution is to mount a lenses with very short focal length on the conventional camera (figure 1.6 (c)). It is the easiest way to enlarge the field of view and the device is quite small.

However, it is very difficult to maintain single viewpoint constraint in this case. Light rays refracted by the fish-eye lenses cannot be converged into a single point. Without single projection center, the pure perspective image cannot be constructed, thus, fish-eye lenses cannot be applied in some vision applications.

Catadioptric Systems The catadioptric systems use a reflective mirror to enlarge the field of view (figure 1.6 (d)). For arbitrary combinations of mirror and camera, catadioptric systems do not always maintain single viewpoint constraint. Only in some special cases, the catadioptric system will maintain the single viewpoint constraint. We call this kind of camera **central catadioptric camera** (alao called single viewpoint catadioptric camera) and the others **non-central catadioptric camera** (also called non-single viewpoint catadioptric camera) that do not satisfy the single viewpoint constraint.

The advantage of catadioptric systems is that they can observe the scene within the field of view in any time. Therefore, it can be applied in the real time applications. With careful alignment of the mirror and the camera, the catadioptric camera can maintain single viewpoint constraint.

The drawback of catadioptric systems is that the size of the device is larger than another two approaches because it needs space to alignment the mirror and camera exactly. Another drawback is that the resolution of the device is lower than the first approach.

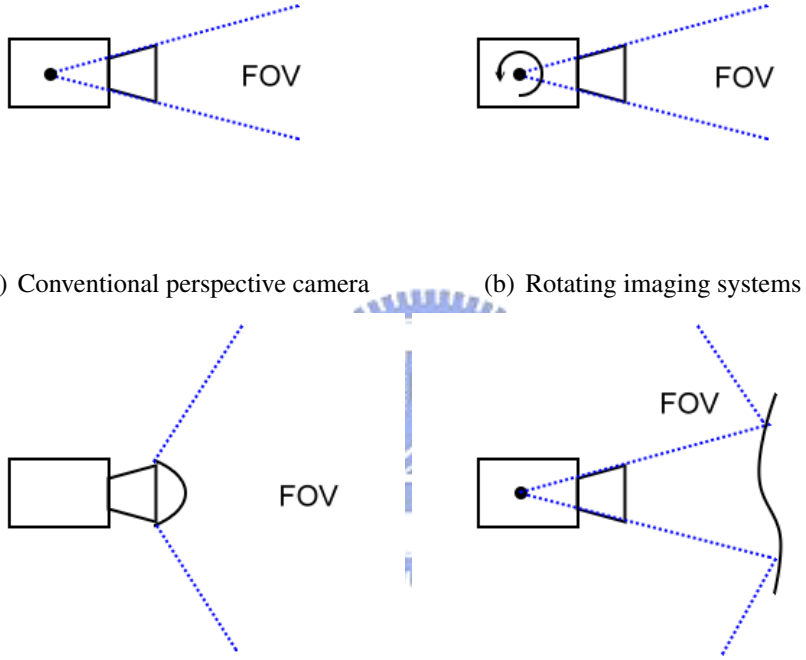

(a) Conventional perspective camera (b) Rotating imaging systems

(c) Fish-eye lenses (d) Catadioptric systems

Figure 1.6: **Methods for enlarging field of view.** (a) Conventional perspective camera has a limited field of view. A larger field of view can be obtained by (b) rotating the imaging system, (b) appending a fish-eye lens to the imaging system, and (d) imaging the scene through a mirror.

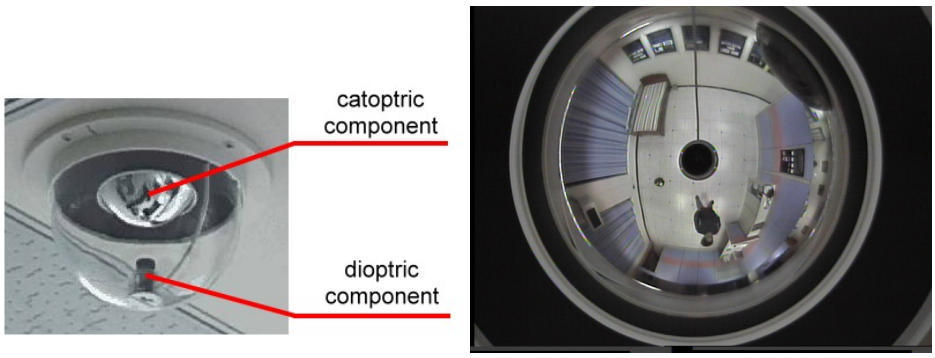

(a) Catadioptric camera (b) Image of catadioptric camera

Figure 1.7: **Catadioptric camera and its image.** The catadioptric camera is composed by two major components, a conventional camera (*catoptric*) and a mirror (*dioptric*).

1.1.3 Catadioptric Camera

After the comparisons in the last section, catadioptric systems seem to be the best solution for enlarging the field of view and still maintaining the property of single viewpoint constraint at the same time. The word "catadioptric" is a combination of two words, **catoptric** and **dioptric**. By the meaning of this word, the catadioptric camera is composed by two major components, the catoptric component which is a conventional perspective camera and dioptric component which is a reflecting mirror (figure 1.7 (a)). By the reflection of the dioptric component, the field of view of the camera is enlarged significantly. The advantage of the large field of view can be applied in many application. Let us take video surveillance for an example. Traditionally, we have to setup many conventional cameras to surveil the entire room, but for catadioptric camera we only need to setup one camera on the ceiling to surveil the same room (figure 1.7 (b)).

Because of the advantage of large field of view, there are many representative implementations of catadioptric imaging systems described in [19, 21, 26, 28, 33, 36]. In 1998, Baker and Nayar [35] show that the only useful physically realizable mirror surfaces of catadioptric cameras that produce a single viewpoint are planar, ellipsoidal, hyperboloidal, and paraboloidal (table 1.1). And the relative position between the camera and the mirror is shown in figure 1.8. For these combinations of camera and mirror, the light rays reflected by the mirror are all converged in a single point (figure 1.9 (a)). This point is the effective

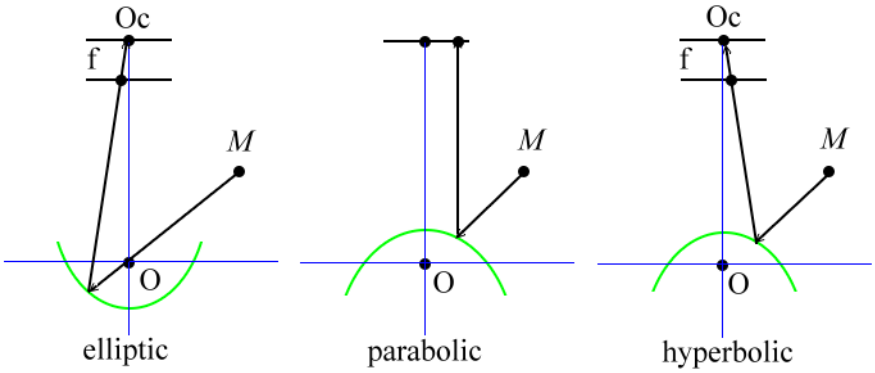

Figure 1.8: **Combinations of central catadioptric cameras.** Four combinations of mirror and camera can maintain the single viewpoint constraint. In the case of elliptic and hyperbolic mirror, the perspective camera must be placed on another focus of the mirror. In the case of parabolic mirror, the image plane of the orthogonal camera must be parallel with the directrix of the parabola. In the case of planar mirror, the perspective camera can be placed arbitrarily.

Combination	Mirror type	Camera type
Type 1	Paraboloidal	Orthogonal camera
Type 2	Planar , Ellipsoidal , Hyperboloidal	Perspective camera

Table 1.1: **Combinations of camera and mirror for central catadioptric camera.**

viewpoint of central catadioptric camera. However, to satisfy some design criterion, such as the size of device, image resolution or field of view, these devices are not necessarily being designed to maintain the single viewpoint constraint, and thus the imaging rays may not pass through a common point. If there is misalignment, the camera cannot maintain the single viewpoint constraint, and the locus of the viewpoints will form a surface, the caustic surface (figure 1.9 (b)).

Camera calibration is a necessary step in 3D computer vision in order to extract the metric information from 2D images. The purpose of the imaging sensor module is to perform a mapping from incoming scene rays to photo-sensitive elements on the image detec-

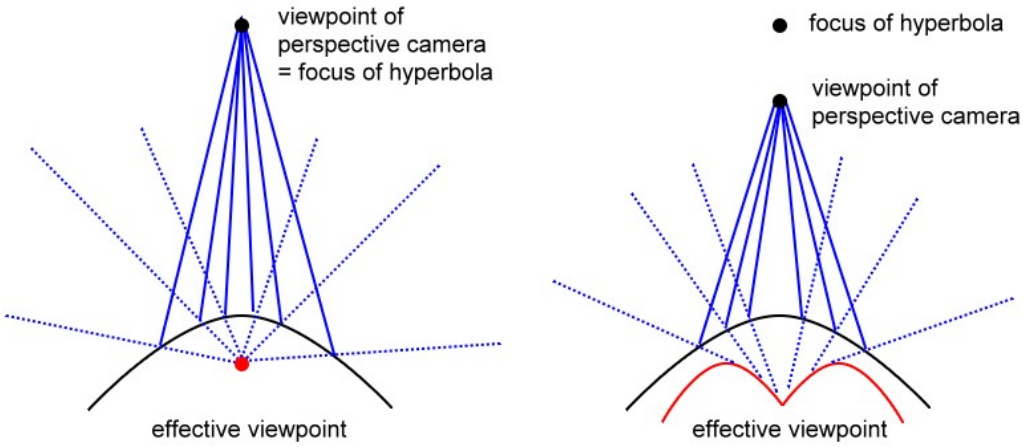

(a) Central catadioptric camera (b) Non-central catadioptric camera

Figure 1.9: **Effective viewpoint of central and non-central catadioptric camera.**

tors. On the contrary, the purpose of camera calibration is to estimate the 3D projection ray of each pixel in the image (figure 1.10). The information that describes the 3D projection ray of each pixel in the image is the camera parameters. The camera parameters include **intrinsic parameters** and **extrinsic parameters**. The extrinsic parameters are the rotation matrix and translation vector which relates the world coordinate to the camera coordinate system; the intrinsic parameters are the projection matrix which relates the camera coordinate to the image coordinate system. Using the intrinsic and extrinsic parameters, we can calculate the 3D projection ray of each pixel in the image, and for any point in space, we can calculate its corresponding pixel in the image.

As aforementioned, catadioptric camera has been widely used in many computer vision applications due to its advantage of large field of view. However, the images acquired by the catadioptric camera are distorted seriously and are not convenient for observation (figure 1.11 (a)). However, if the catadioptric camera is calibrated in advance, the 3D projection ray of each pixel in image can be calculated easily and the virtual perspective and panoramic image [44, 45] can also be rapidly calculated from the original catadioptric image (figure 1.11 (b)). Thus, the drawback of catadioptric camera can be overcame, and

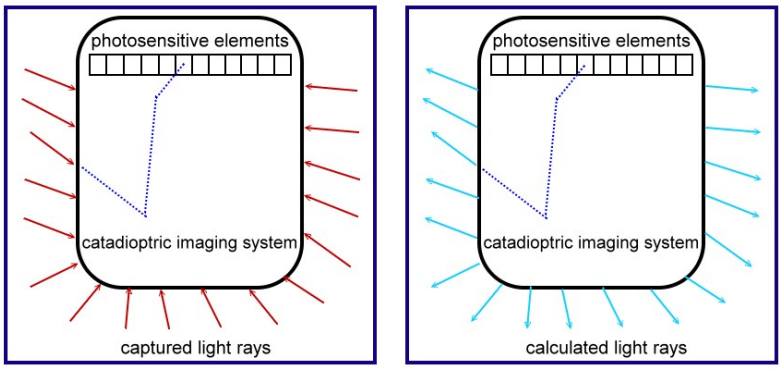

Figure 1.10: **Problem of catadioptric camera calibration.**

this technology is also useful for the future applications such as robot navigation and 3D reconstruction. In another application, we can establish the 3D model of environment easily by using two calibrated catadioptric cameras. For conventional perspective camera, it needs to scan the entire scene many times due to the small field of view. But for catadioptric camera, we only have to capture the image of scene once because of its large field of view.

Another interesting application is to integrate heterogeneous cameras. Although catadioptric cameras have wide field of view, their resolution is much lower than the one of conventional cameras. In another hand, the Pan-Tilt-Zoom (PTZ) cameras have high resolution but their field of view is much narrower than the one of catadioptric cameras. However, there must be occlusion for camera systems at a fixed location. To solve the problem of occlusion, a mobile robot carried a IP camera in the surveillant environment is necessary. These three camera systems have their own advantages and disadvantages. If we can integrate the information of the three camera systems, there will be no blind spots in the surveillant environment.

The catadioptric camera plays an important role in this application. Because of the large field of view, the catadioptric camera can acquire most information of the environment and thus is most suitable to paly an conductor role of the surveillance application. Consequently, the catadioptric camera calibration is such a necessary step to implement this application.

(a) Image of catadioptric camera

(b) Virtual panoramic image

Figure 1.11: **Virtual perspective and panoramic image construction.**
Graph source : http://www1.cs.columbia.edu/CAVE/projects/

(a) Environment of surveillance (b) Image of perspective camera

(c) Image of catadioptric camera (d) Image captured by a mobile robot

Figure 1.12: **Integration of heterogeneous cameras.**

1.2 Thesis Scope

In this thesis, we propose two photogrammetric calibration methods to estimate the intrinsic parameters of central and non-central catadioptric camera systems using planar calibration objects.

For central catadioptric cameras, we propose a novel calibration method using a planar pattern. It only requires the catadioptric camera to observe a planar pattern shown at a few different orientations. Because the central catadioptric camera keeps single viewpoint constraint, the virtual perspective image can be constructed. Therefore, we can estimate the relative pose between virtual perspective camera and calibration pattern to measure the 3D position of all feature points. Then, we can estimate the camera parameters by minimizing the calibration errors on the virtual perspective image plane. Compared with classical techniques which use expensive equipment such as two or three orthogonal planes, the proposed technique is easy to use and flexible.

But for non-central catadioptric cameras, the single viewpoint constraint does not hold. The virtual images calculated from non-central catadioptric image also do not have property of perspective geometry. Hence, we cannot apply the same procedure for non-central catadioptric cameras. We propose a novel calibration method for non-central catadioptric cameras by a calibrated central catadioptric camera and LCD, which is also a planar calibration object. We estimate the 3D position on LCD by a calibrated central catadioptric camera. The LCD also provide correspondence information by displaying a sequence of special patterns. Using the correspondence of 3D points on LCD and 2D points on image plane, we can estimate the camera parameters of non-central catadioptric camera.

In this work, we implemented the proposed methods in C/C++ language on Win32 platform. In the real experiments, we use the **MAPCAM** made by the company EERISE as our non-central catadioptric camera, and the central catadioptric camera is combined by a perspective camera (Marlin F-080C) and the same specification of mirror as the non-central one.

1.3 Thesis Organization

In the next chapter, we will introduce calibration methods for central and non-central catadioptric cameras today. And we also introduce the proposed methods briefly and compare the proposed methods with classical calibration methods. In chapter 3, we introduce the proposed calibration method for central catadioptric cameras using planar calibration objects. At first, we introduce a image formation model for central catadioptric cameras, the viewing sphere model. Next, we describe how to construct a virtual perspective image from a central catadioptric image using an initial parameters of viewing sphere model. Then, we introduce the proposed optimization procedure based on minimizing the distance between estimated and predicted feature points in catadioptric image. In chapter 4, we introduce the proposed calibration method for non-central catadioptric cameras using a calibrated central catadioptric camera and LCD. At first, we propose a method to measure the 3D position of feature points on LCD using a calibrated central catadioptric camera. After estimating the corresponding feature points, we can calibrate the non-central catadioptric camera by minimizing the calibration error. Chapter 5 consists of the results of the experiment for the verification and demonstration of the proposed methods. Finally, a short conclusion for the thesis is given at the last chapter.

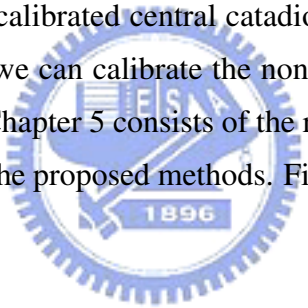

Chapter 2

Survey of Catadioptric Camera Calibration

In this chapter, we review the calibration methods proposed by other researchers for central and non-central catadioptric camera. As aforementioned, the catadioptric camera is composed by a perspective camera and a curved mirror. Hence, it is necessary to review the image formation model and calibration methods for the perspective camera. After reviewing calibration method for perspective camera, we introduce the image formation models of catadioptric camera in the second section. After that, we review the calibration methods for central and non-central catadioptric cameras. Finally, we give an overview of proposed method and compare the proposed method with other calibration methods.

2.1 Review of Perspective Camera Calibration

2.1.1 Image Formation Model for Perspective Camera

The image formation model of perspective camera which is ordinarily used is the **pinhole model** (figure 2.1). Given a world point $\mathbf{M}$ based on arbitrary world coordinate system and its corresponding image point $\mathbf{m}$, we use $\tilde{\mathbf{m}}$ to denote the homogeneous representation of $\mathbf{m}$, use $\tilde{\mathbf{M}}$ to denote the homogeneous representation of $\mathbf{M}$. The relationship of image point $\mathbf{m}$ and $\mathbf{M}$ is given by

$$\lambda\tilde{\mathbf{m}} = \mathbf{K}[\mathbf{R}|\mathbf{t}]\tilde{\mathbf{M}}, \quad \textbf{with} \quad \mathbf{K} = \begin{bmatrix} \alpha & \gamma & u_0 \\ 0 & \beta & v_0 \\ 0 & 0 & 1 \end{bmatrix} \tag{2.1}$$

where λ is an arbitrary scale factor, $[\mathbf{R}|\mathbf{t}]$ called the extrinsic parameters comprising a rotation matrix $\mathbf{R}$ and a translation $\mathbf{t}$ related from the world coordinate system to the camera coordinate system, $\mathbf{K}$ called the intrinsic parameters, with (u_0, v_0), the coordinates of principal point; α and β, the scale factors in image u and v axes; and γ, the parameters describing the skew of two image axes.

2.1.2 Calibration Methods for Perspective Camera Calibration

Camera calibration is a wildly used technique in 3D computer vision. For conventional perspective camera, much work has been done by many researchers. We can classify these

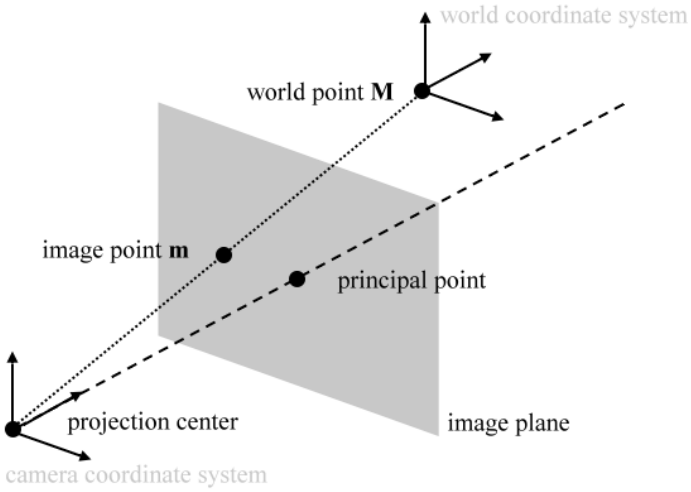

Figure 2.1: **Pinhole model of perspective camera.**

methods into five categories by the dimension of calibration object.

3D calibration object Calibration methods belong to this category [9, 42, 43] are performed by observing a 3D calibration objects which the geometry in 3D space is measured precisely. Calibration using 3D calibration object can be very efficient. However, it always requires an expensive setup before calibration.

2D calibration object Calibration methods which belong to this category [32, 50] only need to observe a planar pattern from a few different view points, and the setup of these methods is very easy.

1D calibration object In 2004, Zhang [51] proposed a calibration method which only needs to observe a 1D calibration object, a stick. The only constraint is that one end of the calibration object needs to be fixed.

0D calibration object In 2005, Chen [25] proposed a calibration method which only needs to observe a 0D calibration object, a ball. In this method, it only needs to throw a ball and the gravity causes the ball falling and generates a parabolic trajectory.

Self calibration Calibration methods in this category [17, 31] do not need any calibration object. They only need to move the camera in a static scene to obtain the image point correspondences. Although no calibration objects are needed, it is difficult to obtain accurate and robust results due to the unstable feature extraction.

Comparison of Calibration Methods for Perspective Camera

There is a tradeoff between the calibration categories of the perspective camera. Calibration methods using 3D calibration object can obtain precise camera parameters. But, these approaches require an expensive calibration apparatus and an elaborate setup. On the other hand, self calibration techniques do not need any calibration object, but the result is not reliable. Thus, there are compromising solutions using 2D,1D or 0D calibration objects [25, 50, 51]. These methods only need a simple setup, and the results are also acceptable. According to different applications, we can choose a suitable calibration method. In our application, Zhang's method using planar calibration object [50] is most suitable. In his method, it only requires perspective camera to observe the planar pattern in a few orientations (at least two), and the intrinsic and extrinsic parameters can be estimated. It is a very flexible method because the motion of the calibration method needs not be known.

2.2 Image Formation Models for Catadioptric Camera

Before the process of calibration, it is necessary to review the image formation model of the camera system. In the first subsection, we will introduce two major image formation models for central catadioptric camera, the **viewing sphere model** and **modified viewing sphere model**. In the second subsection, we will introduce two major image formation models for non-central catadioptric camera, the **reflected ray model** and **caustic model**.

2.2.1 Image Formation Models for Central Catadioptric Cameras

Because central catadioptric cameras keep single viewpoint constraint, the effective viewpoints of light ray reflected by the mirror from a camera will be focus on one single point, one of the two focus of the mirror. Therefore, the image formation of central

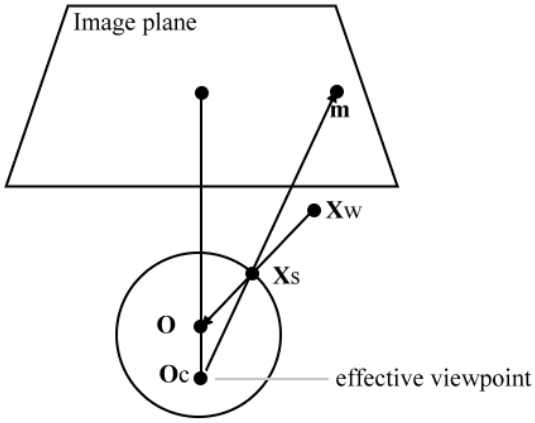

Figure 2.2: **Viewing sphere model.**

catadioptric camera is easier to model than the non-central one.

Viewing Sphere Model

The viewing sphere model is a generalized image formation model for central catadioptric cameras proposed by Geyer and Daniilidis in 2000 [14, 15]. The image model can be applied in central catadioptric camera which is combined by a perspective camera and a planar, ellipsoidal or hyperboloidal mirror, or combined by an orthogonal camera and a parabolic mirror.

Geyer and Daniilidis proved that the central catadioptric image formation is equivalent to a two-step mapping via a sphere:

step 1 : A world point $\mathbf{X_w}$ in 3D space will be projected into a unit sphere centered at the single effective viewpoint (figure 3.1).

The unit sphere is called the viewing sphere. Assuming the point $\mathbf{X_w} = (\mathbf{x_w}, \mathbf{y_w}, \mathbf{z_w})$ in the world coordinate system whose origin is at the single viewpoint, then the corresponding point on the viewing sphere, $\mathbf{X_s} = (\mathbf{x_s}, \mathbf{y_s}, \mathbf{z_s})$ can be calculated by the following equation.

	Ellipsoidal	Paraboloidal	Hyperboloidal	Planar
ε	$0 < \varepsilon < 1$	$\varepsilon = 1$	$\varepsilon > 1$	$\varepsilon \to \infty$
l	$0 < l < 1$	$l = 1$	$0 < l < 1$	$l = 0$

Table 2.1: **Eccentricity ε and distance l in viewing sphere model.**

$$\mathbf{X_s} = (\frac{\mathbf{x_w}}{\|\mathbf{X_w}\|}, \frac{\mathbf{y_w}}{\|\mathbf{X_w}\|}, \frac{\mathbf{z_w}}{\|\mathbf{X_w}\|}) \tag{2.2}$$

step 2 : In this step, we project the point on the sphere $\mathbf{X_s}$ to a point on the image plane $\mathbf{m}$ from the point $\mathbf{O_c}$ (figure 3.1).

This step can be considered as a virtual perspective camera located at $\mathbf{O_c}$ and project points on sphere to the image plane. We have to change coordinate system origin of points on the sphere from $\mathbf{O}$ to $\mathbf{O_c}$. Then, we can calculate the corresponding point on the image plane by the intrinsic matrix of the virtual perspective camera $\mathbf{K}$. Assuming that the distance between $\mathbf{O}$ and $\mathbf{O_c}$ is l, $\mathbf{m}$ can be calculated by following equation.

$$\lambda \mathbf{m} = \mathbf{K} \begin{bmatrix} 1 & 0 & 0 & 0 \\ 0 & 1 & 0 & 0 \\ 0 & 0 & 1 & l \end{bmatrix} \begin{bmatrix} x_s \\ y_s \\ z_s \end{bmatrix} \tag{2.3}$$

For the revolution conic section mirror, it satisfies the following equation $l = \frac{2\varepsilon}{1+\varepsilon^2}$, where ε is the eccentricity of the conic section. The relation between the eccentricity ε and the distance l for different central catadioptric camera is shown in table 2.1.

Modified Viewing Sphere Model

In 2001, Barreto and Araujo [3] also proposed a generalized image formation model for central catadioptric cameras. The image model can be also applied in central catadioptric camera which is combined by a perspective camera and a planar, ellipsoidal or hyperboloidal mirror, or combined by an orthogonal camera and a parabolic mirror.

The central catadioptric image formation proposed by Barreto and Araujo can be described in four steps (figure 2.3).

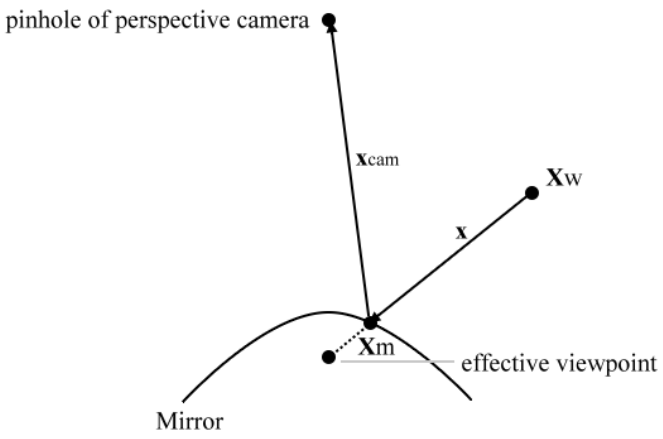

Figure 2.3: **Modified viewing sphere model.**

step 1 : Calculate the incoming ray $\mathbf{x}$ from a world point $\mathbf{X_w}$ to the effective viewpoint.

Given a world point $\mathbf{X_w}$, we can calculate the incoming ray $\mathbf{x} = \mathbf{R}[\mathbf{I}| - \mathbf{C}]\mathbf{X_w^h}$, where $\mathbf{X_w^h}$ is the homogeneous representation of $\mathbf{X_w}$, $\mathbf{R}$ is the rotation matrix the coordinate systems, $\mathbf{C}$ is the origin of world coordinate in mirror coordinate system and $\mathbf{I}$ is a 3×3 identity matrix.

step 2 : Calculate the intersection point $\mathbf{X_m}$ of the incoming ray $\mathbf{x}$ and the mirror surface.

Every point on the incoming ray $\mathbf{x}$ can be represented by $\lambda\mathbf{x}$. The intersection point $\mathbf{X_m}$ of the incoming ray $\mathbf{x}$ and the mirror surface can be calculated by $\mathbf{X_m} = \lambda\mathbf{x}$, where λ is presented in (table 2.2).

step 3 : Calculate the reflecting ray $\mathbf{x_{cam}}$ from the intersection point $\mathbf{x_m}$ to the pinhole of perspective camera.

The corresponding reflecting ray can be calculated by $\mathbf{X_{cam}} = \mathbf{P_c}\mathbf{A_c}\mathbf{X_M^h}$, where $\mathbf{A_c}$ is a 4×4 transformation matrix between mirror and camera coordinate systems, $\mathbf{P_c}$ is a 3×4 projection matrix. For hyperbolic, elliptical and planar catadioptric systems, $\mathbf{P_c}$ is a perspective projection matrix, and for parabolic catadioptric systems, $\mathbf{P_c}$ is a orthogonal

	λ	$\mathbf{P_c}$	$\mathbf{R_c}$
Parabolic	$\frac{2p}{z+r}$	$\begin{bmatrix} 1 & 0 & 0 & 0 \\ 0 & 1 & 0 & 0 \\ 0 & 0 & 0 & 1 \end{bmatrix}$	$\mathbf{I}$
Hyperbolic	$\frac{2dp}{z(\sqrt{d^2+4p^2}+2p)+dr}$	$[\mathbf{I}\|\mathbf{0}]$	any
Elliptical	$-\frac{2dp}{z(\sqrt{d^2+4p^2}-2p)+dr}$	$[\mathbf{I}\|\mathbf{0}]$	any
Planar	$\frac{d}{2z}$	$[\mathbf{I}\|\mathbf{0}]$	any

Table 2.2: **Parameters of modified viewing sphere model.**

projection matrix (table 2.2).

step 4 : Calculate the corresponding image point $\mathbf{x_i}$ of the reflecting ray $\mathbf{x_{cam}}$.

The image point can be calculated by the following equation $\mathbf{x_i} = \mathbf{K_c}\mathbf{R_c}\mathbf{x_{cam}}$, where $\mathbf{K_c}$ is the intrinsic parameters of perspective camera, R_c is a rotation matrix. For the combination of perspective camera and hyperbolic, elliptical or planar mirror, R_c can be an arbitrary rotation matrix. If the lenses center of the perspective camera is placed on the another focus of the mirror, the single viewpoint constraint will be reserved. However, for the combination of orthogonal camera and parabolic mirror, the image plane of orthogonal camera must be orthogonal to the axis of parabolic mirror, that is R_c is an identity matrix.

In the work of Barreto and Araujo, they proved that their image model is also equivalent to a mapping via a sphere. Compared the method proposed by Barreto and Araujo and the viewing sphere model, the concept of image formation models are similar. But in details, the parameters of their model are quite different. The both models are used in the future calibration methods and the detail will be described in next section.

2.2.2 Image Formation Models for Non-central Catadioptric Cameras

Because non-central catadioptric cameras do not maintain single viewpoint constraint, the viewpoints of light rays reflected by mirror from camera will focus on a caustic surface rather than a single point. Thus, the image formation of non-central catadioptric camera is

much complicate than the central one. In this section, we introduce two image formation models for non-central catadioptric camera, **reflected ray model** and **caustic model**.

Reflected Ray Model

Because non-central catadioptric cameras do not maintain single viewpoint constraint, given a world point, we can not calculate the corresponding point on the mirror surface. Hence, there is no close form solution for forward image model for non-central catadioptric camera. We have to derive the image formation model from image point rather than a world point.

Much work has been done in the work. In 2001, Swaminathan et. al. [40] proposed a method to find the caustic surface for non-central catadioptric cameras. In his method, he use the geometry of the reflector,i.e. *the angle between incoming vector and normal vector equals the angle between normal vector and reflected ray*. In 2004, Micusik et. al. [38] proposed a image formation model for non-central catadioptric camera which combined a perspective camera and a sphere, parabolic or hyperbolic mirror. Later on, Mashita et. al. [48] also proposed a image formation method for non-central catadioptric camera composed by a perspective camera and a hyperbolic mirror in 2005.

Here, we introduce backward image formation model proposed by Mashita et. al. The image formation can be described in four steps as following (figure 2.4).

step 1 : Calculate the corresponding ray $\mathbf{V_c}$ from an image point $\mathbf{x}$.

The corresponding ray $\mathbf{V_m}$ from image point $\mathbf{x}$ can be calculated by the following equation $\mathbf{V_c} = \lambda\ \mathbf{K}^{-1}\tilde{\mathbf{x}}$, where $\mathbf{K}$ is the intrinsic matrix of the perspective camera, $\tilde{\mathbf{x}}$ is the homography representation of $\mathbf{x}$.

step 2 : Change the coordinate system of $\mathbf{V_c}$ from perspective camera coordinate system to mirror coordinate system $\mathbf{V_m}$.

Given a transformation matrix $[\mathbf{R}|\mathbf{t}]$ between the coordinate system of camera and the one of mirror, we can calculate $\mathbf{V_m}$ by the equation $\mathbf{V_m} = [R|t]\mathbf{V_c}$.

step 3 : Calculate the intersection point of incoming ray $\mathbf{V_m}$ and the mirror surface.

Every point on the incoming ray can be represented by $\mathbf{F_m} + \mathbf{kV_m}$. The intersection point $\mathbf{X_m}$ of the incoming ray $\mathbf{x}$ and the mirror surface can be calculated by solving the

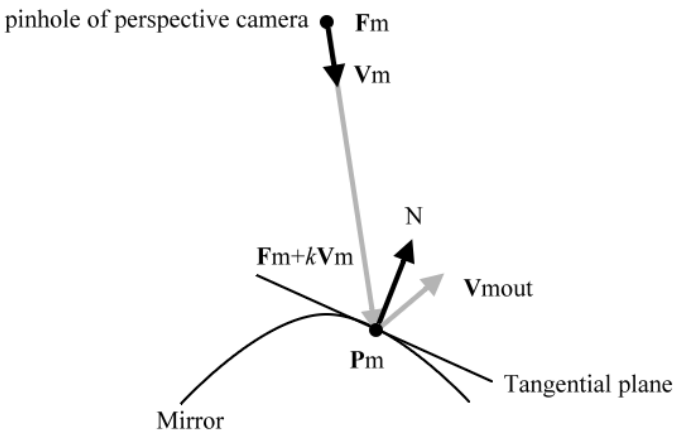

Figure 2.4: **Reflected ray model.**

parameter k. Assuming a and b are the parameters of the hyperbolic mirror, k can be calculated by the following equations.

$$k = \frac{-\beta_M + \sqrt{{\beta_M}^2 - \alpha_M \gamma_M}}{\alpha_M} \tag{2.4}$$

$$\alpha_M = \frac{V_{MX}^2 + V_{MY}^2}{a^2} - \frac{V_{XZ}^2}{b^2} \tag{2.5}$$

$$\beta_M = \frac{V_{MX}F_{MX} + V_{MY}F_{MY}}{a^2} - \frac{V_{MZ}F_{MZ}}{b^2} \tag{2.6}$$

$$\gamma_M = \frac{F_{MX}^2 + F_{MY}^2}{a^2} - \frac{F_{MZ}^2}{b^2} + 1 \tag{2.7}$$

step 4 : Calculate the reflected ray $\mathbf{V_{Mout}}$ using the geometry of the reflector.

Before the calculation of reflected ray, we need to calculate the normal vector $\mathbf{N}$ of the point $\mathbf{X_m}$ on mirror surface. The mirror surface can be describe in the following equation.

$$f(X_M, Y_M) = Z = \sqrt{b^2(\frac{X_M^2 + Y_M^2}{a^2} + 1)} \tag{2.8}$$

The normal vector $\mathbf{N}$ can be calculated by following equation.

$$\mathbf{N} = (\mathbf{f_{XM}}((\mathbf{P_M})), \mathbf{f_{YM}}((\mathbf{P_M})), -\mathbf{1}) \tag{2.9}$$

Next, using the geometry of reflector, the reflected ray $\mathbf{V_M out}$ can be calculated by the following equation.

$$\mathbf{V_{Mout}} = \mathbf{V_M} - \mathbf{2N}(\mathbf{N}, \mathbf{V_M}) \tag{2.10}$$

Applying above process, we can obtain backward image formation model of non-central catadioptric cameras, i.e. given a image point on catadioptric image plane, we can estimate its corresponding light ray in 3D space.

However, there is no close form solution for forward image formation for non-central catadioptric camera because it does not maintain single viewpoint constraint. We have calculate the backward image formation by an iterative method. Given a world point $\mathbf{X_m}$ in 3D space, we want to estimate its corresponding image point $\mathbf{x}$ on catadioptric image plane. At first, we can estimate an initial image point $\mathbf{x_{initial}}$ of $\mathbf{X_m}$ by central catadioptric forward image formation model. Next, we use a iterative method to minimize the distance between the ray of $\mathbf{x_{initial}}$ calculated by non-central backward image formation, and the world point $\mathbf{X_m}$. Finally, we can obtain the corresponding image point $\mathbf{x}$ of the world point $\mathbf{X_m}$.

Caustic Model

As aforementioned, the viewpoints of non-central catadioptric camera is a caustic surface rather than a single viewpoint. In 2001, Swaminathan et. al. proposed a method to find the caustic surface of non-central catadioptric cameras using the reflected ray model. The physical meanings of caustics is the place that light rays most converge or the locus of the viewpoints (figure 2.5).

Using the reflected ray model, we can obtain the geometrical property of non-central catadioptric camera. Why do we need to calculate the caustics? In Swaminathan's work,

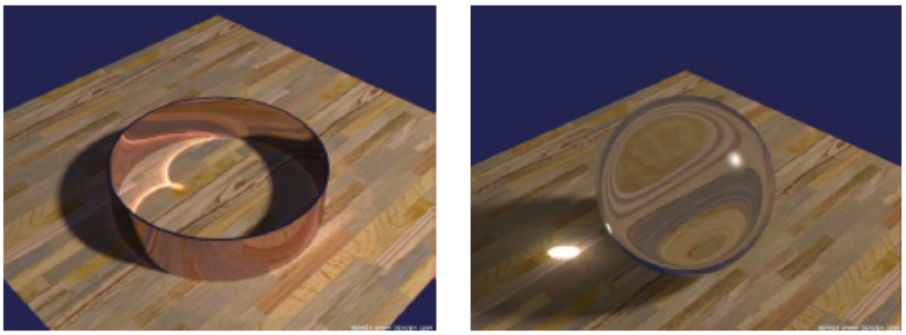

Figure 2.5: **An example of the caustic.** Bright patterns of light on the table illustrate a section of the caustic surface formed. The caustics is the place where light rays most converge, and it is also the locus of viewpoints.
Graph source : http://graphics.stanford.edu/ henrik/ images/caustics.html

Property	Caustic model	Reflected ray model
Geometric property	O	O
Radiometric property	O	X
Optical property	O	X
Calculation	X	O

Table 2.3: **Comparisons of image models for non-central catadioptric camera.**

they mention that the study of caustics can help us to understand not only the geometry property but also the radiometrical and optical properties, such as field of view and resolution of the cameras. However, it is a time consuming work to calculate the caustic surface due to the calculation of Jacobian (table 2.3). Thus, using the reflected ray model is enough if we only need to obtain the geometrical information of non-central catadioptric camera.

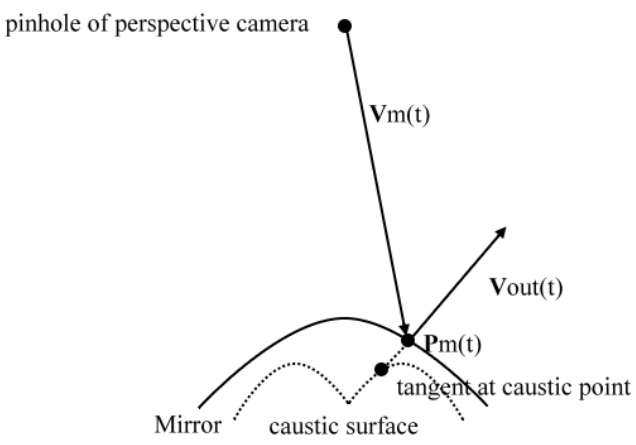

Figure 2.6: **Caustic surface of non-central catadioptric camera.**

2.3 Relative Works of Central Catadioptric Camera Calibration

Catadioptric camera has been widely used in many computer vision applications recently. Much work has been done for catadioptric camera calibration. Calibration methods for catadioptric camera can be classify into three categories, **photogrammetric calibration**, **geometric invariant** and **self calibration**.

Because central catadioptric cameras have a single center of projection, there are many properties can help us calibrate the central catadioptric camera. Such as the epipolar geometry can be applied in central catadioptric camera, some geometric properties are preserved in central catadioptric images, and we can also compute pure perspective image from original catadioptric image.

Self Calibration Same with the perspective camera, calibration methods which belong to this category do not need calibration objects. They only use points correspondence in multiple view. But, it is well known that stereo correspondence estimation is a

Calibration category	Camera Type	Group	Calibration method
Self-calibration	Type 1	Kang (CVPR 2000)	Mirror boundary
Self-calibration	Type 1	Micusik (ACCV 2004)	Epipolar constraint
Geometry invariant	Type 1	Geyer (PAMI 2002)	Projection of lines
Geometry invariant	Type 1,2	Barreto (PAMI 2005)	Projection of lines
Geometry invariant	Type 1,2	Ying (PAMI 2004)	Projection of lines or sphere

Table 2.4: **Relative works of central catadioptric camera calibration.**

difficult problem in computer vision.

There is much work have been done for catadioptric camera calibration by using self-calibration methods. For example, Kang [27] proposed a self-calibration method by using the mirror boundary in image for para-catadioptric cameras. Micusik and Pajdla [39] also proposed a self-calibration method from point correspondences in two views based on the epipolar constraint.

Geometric invariants Because central catadioptric cameras maintain single viewpoint constraint, the property of perspective geometry can be used in the calibration, and this kind of method do not need any metric information.

Geyer and Daniilidis [13, 16] proposed a calibration method for intrinsic parameter of catadioptric camera by geometry invariants of space lines for para-catadioptric cameras. They also [14] proposed a viewing sphere model for generalized central catadioptric cameras in 2000. Then, Barreto et. al. [4, 6] and Ying et. al. [22, 24] proposed the calibration methods using modified viewing sphere model and viewing sphere model. Barreto calibrated catadioptric camera using three lines in space and Ying did it using three lines or two spheres in space.

Comparison of Calibration Methods for Central Catadioptric Camera

As aforementioned, the central catadioptric camera can be composed in different type of mirrors and cameras. Some calibration methods [16, 27, 39] can only applied in the

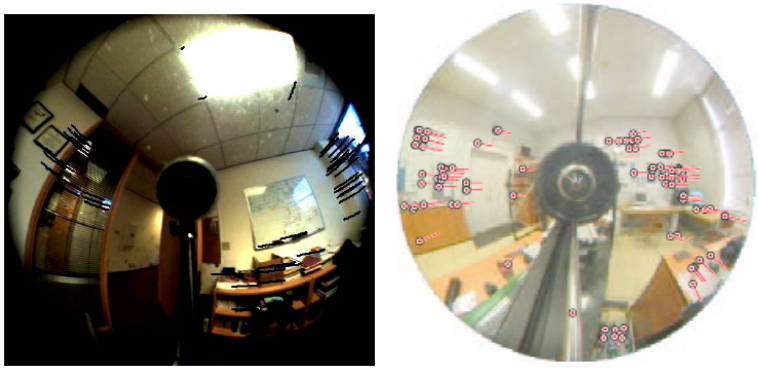

(a) Kang's method (b) Pajdla's method

Figure 2.7: **Self-calibration for central catadioptric camera.** Calibration methods which belong to this category do not need calibration objects [27, 39]. They only use points correspondence in multiple view. But, it is well known that stereo correspondence estimation is a difficult problem in computer vision.

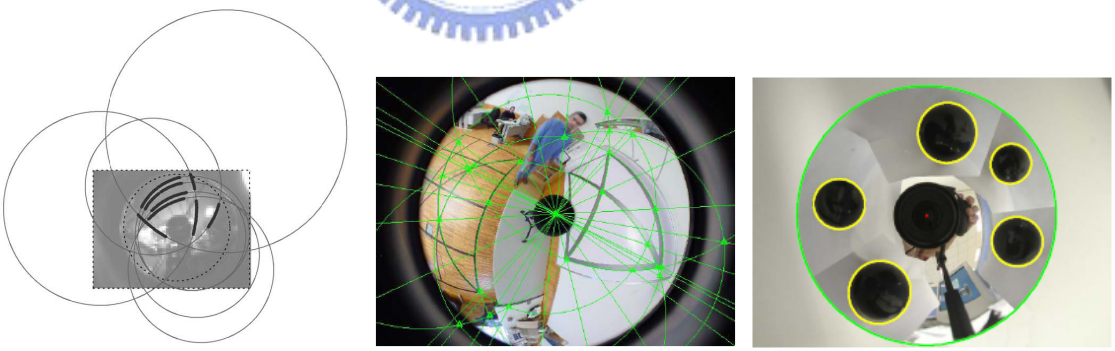

(a) Daniilidis's method (b) Araujo's method (c) Ying's method

Figure 2.8: **Calibration methods using geometric invariants for central catadioptric camera.** Calibration methods which belong to this category estimate camera parameters using the geometry properties of space line and sphere [4, 6, 13, 16, 22, 24].

combination of orthogonal camera and parabolic mirror (type 1), thus, the application of these approaches are limited. Methods using generalized image formation models [4,6,24] can be applied in all combinations of central catadioptric cameras. These methods all use the property of geometry invariants to calibrate the central catadioptric camera. According to the work of Ying and Hu [24], the performance using sphere images is better than the one using line images. Although lines and spheres are all projected into a conic in the image plane, it is more difficult to extract the projection of a line with high accuracy than that of a sphere. The projection of a line on the image is a partial conic (e.g. about one-third of an ellipse), and conic fitting using points lying on a portion of a conic is an error-prone process. The projection of a sphere on the image is a complete conic. Therefore, sphere images are preferred in the case where accurate calibration of central catadioptric cameras is needed. The most important contribution of his work is to introduce spheres for the central catadioptric camera calibration. Therefore, we briefly describe the state of the art, **Catadioptric Camera Calibration using Geometric Invariants** as following.

Ying and Hu use lines or sphere in 3D space as calibration objects. Viewing sphere model is used in this method, thus it can be applied in all kinds of central catadioptric cameras. By using viewing sphere model, they derive two invariants for sphere image and three invariants for line image. They proposed a two-step calibration method by these invariants. First, they estimate an initial parameters of viewing sphere model using the mirror boundary. Second, they optimize the parameters by minimizing the constraint they derived.

2.4 Relative Works of Non-central Catadioptric Camera Calibration

For non-central catadioptric cameras, the single viewpoint constraint does not hold. Therefore, we can not calibrate non-central catadioptric camera using geometric invariants. There are only two categories for calibration methods for non-central catadioptric camera.

Photogrammetric calibration This kind of methods use a calibration object with control points which 3D coordinate is known. Using iterative methods, extrinsic parameters

(position and orientation) and intrinsic parameters can be recovered.

Aliaga [2] relaxed the assumption of the perfect orthographic projection and replacement. But it only compensates for minor misalignment between perspective camera and mirror. Strelow et. al. [41] proposed a model for relation between the mirror and camera with 6 degrees of freedom (translation and rotation). They determined 6 parameters through nonlinear optimization. This method has the advantage that the translation and rotation parameters are simultaneously determined. But the disadvantage is that the accuracy of the estimated parameters is worse and depends on the initial values because of the nonlinear optimization.

Beside the above methods, Grossburg and Nayar [34] proposed a calibration method for general imaging devices. In their method, he considered the general imaging device as a black box. There will be a lookup table to store the 3D projection ray of each pixel in the image. Although this method is general and can be applied in arbitrary imaging device, the parameters estimated by the method are not accurate enough.

Self Calibration Micusik [5] proposed a self-calibration method using the mirror boundary and the epipolar constraint. However, it also compensates for minor misalignment between perspective camera and mirror. To overcome the disadvantage of Strelow's method, Mashita [48] proposed a new method to find the relation between mirror and camera by using the mirror boundary.

Comparison of Calibration Methods for Non-central Catadioptric Camera

For non-central catadioptric cameras, there are some approaches [2, 39] using central image formation model to approximate non-central image formation model. Because of the approximation of central projection, these two methods only compensate for minor misalignment. To compensate large misalignment, we have to model non-central catadioptric camera by separating the camera model and the mirror model. Methods [41, 48] using this model can compensate large misalignment between mirror and camera. The key of the two methods is to find the relative position between perspective camera and mirror, then

Calibration category	Camera type	Group	Calibration method
Photogrammetric calibration	Type 1	Aliaga (ICCV 2001)	Known 3D points coordinate
Photogrammetric calibration	Type 2	Strelow (CVPR 2001)	Known 3D points coordinate
Photogrammetric calibration	Arbitrary camera	Grossburg (ICCV 2001)	Lookup table
Self-calibration	Type 2	Micusik (CVPR 2004)	Epipolar constraint
Self-calibration	Type 1,2	Mashita (OMVI 2005)	Mirror boundary

Table 2.5: **Relative works of non-central catadioptric camera calibration.**

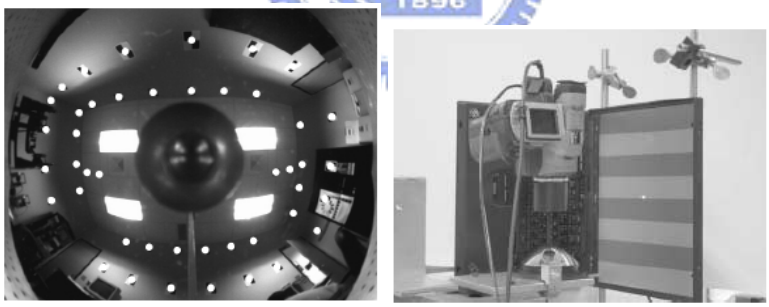

(a) Strelow's method (b) Nayar's method

Figure 2.9: **Photogrammetric calibration for non-central catadioptric camera.** Calibration methods which belong to this category estimate camera parameters by using calibration objects with control points which 3D coordinate is known [2, 34, 41]. The calibration is efficient, but it requires an expensive calibration apparatus and an elaborate setup.

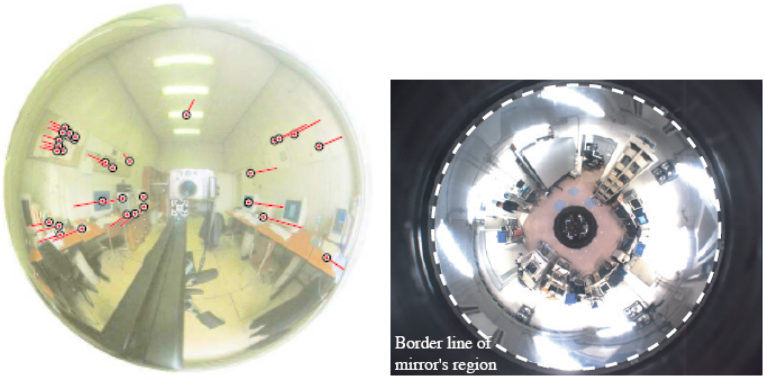

(a) Pajdla's method (b) Mashita's method

Figure 2.10: **Self-calibration for non-central catadioptric camera.** Calibration methods which belong to this category do not need calibration objects [5, 48]. But the calibration result is not stable.

using light tracking to connect the image formation model of perspective camera and the reflecting model of mirror. In the work of Mashita et. al. [48], they show that the performance of their method is better than the one of Micusik's method. Therefore, we briefly describe the state of the art, **Calibration Method for Misaligned Catadioptric Camera** as following.

In Mashita's method, the image formation model is the reflected ray method. In this model, the models of perspective camera and the mirror are separated and there is a transformation matrix to represent the mirror posture. They estimate the mirror posture by the mirror boundary in the catadioptric image. The mirror posture estimated by their method has four solutions. They also propose a mirror posture selection method using line at infinity.

2.5 Overview of Our Methods

In this thesis, we proposed a calibration method for central catadioptric camera using a planar calibration object. We also proposed a calibration method for non-central catadioptric camera using a calibrated central catadioptric camera and LCD. Both of the calibration methods are photogrammetric calibration method.

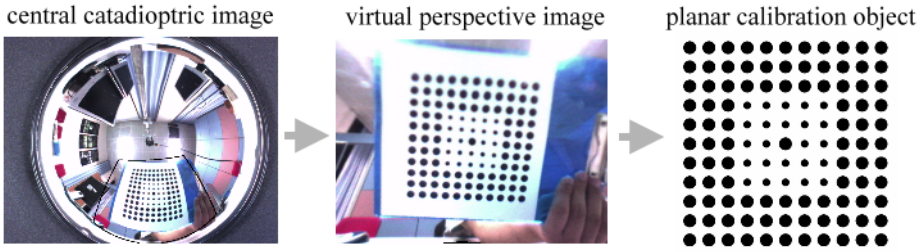

Figure 2.11: **Concept of proposed calibration method for central catadioptric camera.**

As aforementioned, central catadioptric camera keeps the single viewpoint constraint, thus the virtual perspective image can be constructed. If the estimated parameters of camera is correct, the constructed virtual perspective image is more like real perspective image. The intuitive concept of the proposed calibration method for central catadioptric camera is to estimate a set of parameters such that the virtual perspective image is most like real perspective image (figure2.11). In real implementation, we use a planar pattern as our calibration object and minimize the calibration error on virtual perspective image of calibration pattern to obtain the precise camera parameters.

In the procedure of central catadioptric camera calibration, we only have to place a planar pattern in front of the central catadioptric camera in a few orientations. The processes of capturing images of planar pattern are the more the better, and it is better to place the pattern in every orientation of central catadioptric camera. Because the constructed virtual image is perspective image, we can estimate the relative pose between virtual perspective camera and the planar pattern by using Zhang's pose estimation method [50]. Therefore, the motion of the planar pattern need not to know.

For non-central catadioptric camera, we cannot obtain the 3D position of feature points on the calibration object by above method, because the single viewpoint constraint does not hold for non-central catadioptric camera and we cannot construct virtual perspective images. For photogrammetric calibration methods, it is very important to measure precise

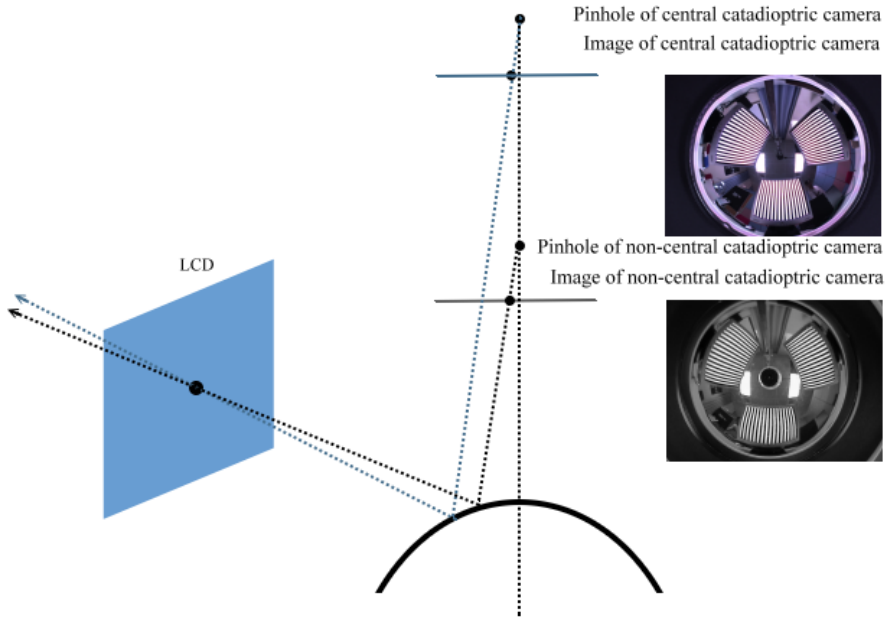

Figure 2.12: **Concept of proposed calibration method for non-central catadioptric camera.** We use a calibrated central catadioptric camera to estimate precise 3D position of feature points on calibration pattern, a LCD.

3D position of calibration object, however it is very difficult to measure precise 3D position of features points for catadioptric camera because of its large field of view. Besides, the correspondence between 3D world points and 2D image points are estimated manually. In order to solve these two problems, we use a calibrated central catadioptric camera to estimate precise 3D position of feature points on calibration pattern, a LCD (figure2.12). The correspondence between 3D world points and 2D image points is provided by displaying 20 different patterns on LCD (figure2.13). By using the correspondence between 3D world points and 2D image points, we can estimate the camera parameters by minimizing distance between the light ray calculated from image point and the 3D point estimated by the calibrated central catadioptric camera.

There is also a tradeoff between the calibration categories of the catadioptric camera. Calibration methods using photogrammetry can obtain precise camera parameters. But, these approaches require an expensive calibration apparatus and an elaborate setup to mea-

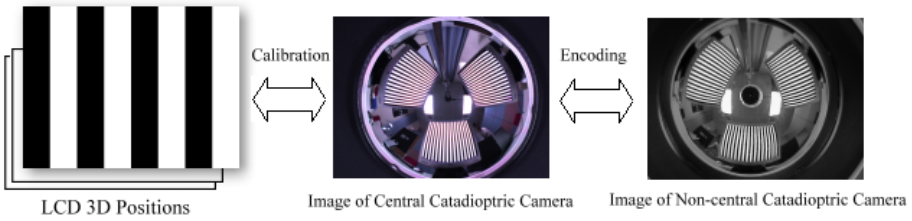

Figure 2.13: **Correspondence estimation between central and non-central catadioptric images.** The correspondence between 3D world points and 2D image points is provided by displaying 20 different patterns on LCD.

sure precise coordinate of 3D points. On the other hand, self calibration techniques do not need any calibration object, but the result is not reliable. Between these two categories, some calibration methods use the geometric invariants of space line and sphere to estimate camera parameters, and its calibration result is acceptable.

Compared with classical photogrammetric calibration methods, our method does not need any expensive calibration apparatus and an elaborate setup. It only requires the catadioptric camera to observe a planar pattern shown at a few different orientations. The pattern can be printed on a laser printer and attached to a reasonable planar surface. Therefore, our method is more flexible and easy to use; Compared with classical self-calibration methods, the calibration result of our method should be better theoretical due to precise feature extraction; Compared with classical calibration methods using geometric invariants, the advantages of these methods are that they do not have to give correspondence between 2D image points and 3D world points, and do not have to estimate the transformation between world and camera coordinate systems. However, the two problems are both solved in our proposed method, and the experiment results show that the performance of proposed method is better.

Through the above comparison, it shows that our method is flexible and easy to use than classical calibration methods. In following chapters, we will introduce our methods in detail. We also prove that our calibration methods is accurate and robust, and the performance of our method for central catadioptric camera is better than calibration methods

using geometric invariants in real experiment.


E
S
A
1896

Chapter 3

Central Catadioptric Camera Calibration using a Planar Calibration Object

In this chapter, we introduce the proposed calibration method for central catadioptric camera using planar calibration objects. First, we introduce a general image formation model for central catadioptric camera, the viewing sphere model (VSM). After that, we estimate the initial catadioptric camera parameters by combining the parameters of its components, including the perspective camera and the hyperboloidal mirror. At last, we introduce an optimization method for refining the parameters of central catadioptric camera.

3.1 Image Formation Model for Central Catadioptric Camera

In many image formation models of central catadioptric camera, the viewing sphere model is the most general one of these models because it can be applied by the catadioptric camera which combines the perspective camera and many kinds of mirror (planar, parabolic and hyperbolic mirrors). Hence, we choose the viewing sphere model as our image formation model. The image formation equation of VSM is as following.

$$\lambda \mathbf{p} = \mathbf{K}[\mathbf{R}|\mathbf{t}]\mathbf{x}_{\mathbf{sphere}}, \tag{3.1}$$

Above is a simplified equation, and the complete equation is as following.

$$\lambda \begin{bmatrix} x_i \\ y_i \\ 1 \end{bmatrix} = \begin{bmatrix} rf_e & s & u_0 \\ 0 & f_e & v_0 \\ 0 & 0 & 1 \end{bmatrix} \begin{bmatrix} 1 & 0 & 0 & 0 \\ 0 & 1 & 0 & 0 \\ 0 & 0 & 1 & l \end{bmatrix} \begin{bmatrix} x_s \\ y_s \\ z_s \\ 1 \end{bmatrix} \tag{3.2}$$

In the viewing sphere model, a world point, $\mathbf{x}_{\mathbf{world}}$, is projected into an unit sphere, called **viewing sphere**, and $\mathbf{x}_{\mathbf{sphere}}$ is the corresponding point of original world point on viewing sphere. We change the coordinate system of $\mathbf{x}_{\mathbf{sphere}}$ from viewing sphere coordinate system into catadioptric camera coordinate system by multiplying the matrix $[\mathbf{R}|\mathbf{t}]$, which is a transformation matrix. Next, we project the points on the viewing sphere into the image plane of catadioptric camera by multiplying a projection matrix $\mathbf{K}$. Finally, we can obtain that the original world point, $\mathbf{x}_{\mathbf{world}}$ is projected to point, $\mathbf{p}$ on the image plane.

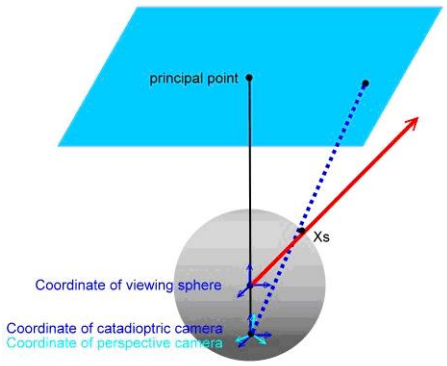

Figure 3.1: **Viewing sphere model.** In the image model, a world point is projected into a unit sphere first, called the viewing sphere. We change the coordinate system of the point from viewing sphere system into the catadioptric camera coordinate system. At last, the point on the viewing sphere is projected into the image plane. And we can obtain the corresponding point on the image plane of the original world point. In the contrary, we can calculate the 3D projection ray of each pixel in the image.

In other words, a point on the image plane, $\mathbf{p}$, is projected into a light ray in 3-D space and this light ray passes the point, $\mathbf{x}_{\mathbf{world}}$ (figure 3.1).

In the viewing sphere model, there are six parameters for image formation, f_e, r, s, u_0, v_0 and l, where f_e is the effective focal length of the central catadioptric camera; r is the aspect ratio; s is the skew factor; u_0 and v_0 are the coordinate of principal point. The meanings of above five viewing sphere parameters are the same with the perspective ones. Besides the parameter l, this parameter will be related with the specification of the hyperboloidal mirror, i.e. the eccentricity of the hyperboloid. Through the viewing sphere model, we can calculate the 3D projection ray of each pixel in the image of central catadioptric image. For every point in the space,we can easily calculate its corresponding pixel on catadioptric image plane.

3.2 Initial Estimation of Viewing Sphere Model Parameters

In this section, we estimate an initial parameters for viewing sphere model. According Ying's work [23], we can get the initial parameters of viewing sphere model by combining the parameters of perspective camera and hyperboloidal mirror if the central catadioptric camera is aligned perfectly (figure 3.2). The calculation of the parameters are as following. The principal point (u_0, v_0), skew factor s and aspect ratio r of viewing sphere model are the same with the perspective camera; and the translation l can be derived by the eccentricity of hyperboloid ε using the following equation $l = \frac{2\varepsilon}{1+\varepsilon^2}$, the effective focal length f_e of viewing sphere model must be estimated by combining the focal length of perspective camera and eccentricity of hyperboloid by the following equation $f_e = -\frac{1-\varepsilon^2}{1+\varepsilon^2} f$. Putting them all together, we can obtain an initial parameter of central catadioptric camera.

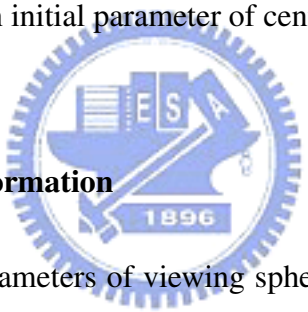

Forward and backward image formation

After estimating the initial parameters of viewing sphere model, we can calculate the 3D projection light ray for each pixel in the image. We can derive the equation of **forward image formation** from the viewing sphere model as following [29].

$$\begin{cases} x_i = \frac{r f_e x_s + s y_s + u_0 z_s + u_0 l}{z_s + l} \\ y_i = \frac{f_e y_s + v_0 z_s + v_0 l}{z_s + l} \end{cases} \tag{3.3}$$

In the same way, we want to derive the equation of **backward image formation** from the viewing sphere model. But in this case, there are four variables, x_s, y_s, z_s and λ and we only have three equations. We need one more equation to solve four variables. Because x_s, y_s and z_s are all on the viewing sphere, we can introduce one equation, the viewing sphere constraint. Then, we have enough equation and can derive the equation of backward formation.

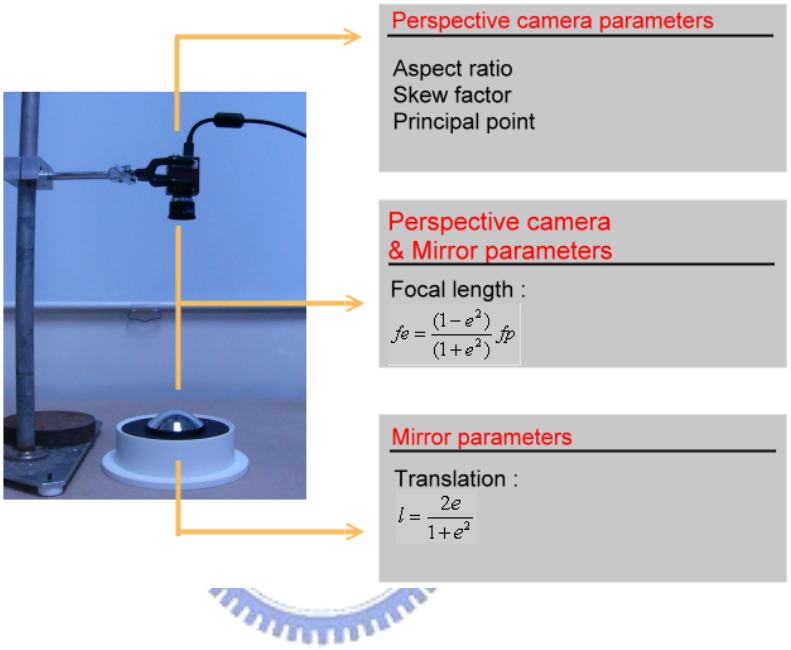

Figure 3.2: **Initial estimation of parameters in viewing sphere model.** By combining the parameters of perspective camera and hyperboloidal mirror, we can get the initial parameters of viewing sphere model. The principal point (u_0, v_0), skew factor s and aspect ratio r of viewing sphere model are the same with the perspective camera. The translation l can be derived by the eccentricity of hyperboloid. The effective focal length of viewing sphere model must be estimated by combining the focal length of perspective camera and eccentricity of hyperboloid. Finally, we can obtain the initial parameters of central catadioptric camera.

$$\begin{cases} x_s = \frac{\lambda(f_e(x_i - u_0) - s(y_i - v_0))}{r f_e^2} \\ y_s = \frac{\lambda(y_i - v_0)}{f_e} \\ z_s = \lambda - l \\ x_s^2 + y_s^2 + z_s^2 = 1 \\ \text{(viewing sphere constraint)} \end{cases} \tag{3.4}$$

$$\begin{cases} x_s = \lambda x' \\ y_s = \lambda y' \\ z_s = \lambda - l \\ \lambda = \frac{l + \sqrt{x'^2(1-l^2) + y'^2(1-l^2) + 1}}{x'^2 + y'^2 + 1} \end{cases} \tag{3.5}$$

Virtual perspective image construction

After introducing the equations of forward and backward formation, we can calculate the virtual perspective image of central catadioptric image (figure 3.3). We can select a point of interest $\mathbf{m_0}$ from original catadioptric image and calculate the corresponding 3D light ray $\mathbf{m_s}$ by the backward equation. Then, we can set the intrinsic parameters of the virtual perspective camera and get the virtual image plane. For every pixel on the virtual image plane, we can calculate the corresponding point on viewing sphere by normalizing the vectors. Then, we change the coordinate system of the points from virtual perspective camera to the one of viewing sphere by multiplying a transformation ${}^{sphere}\mathbf{T}_{perspective}$.

$${}^{sphere}\mathbf{T}_{perspective} = \begin{bmatrix} \mathbf{x_{sx}} & \mathbf{x_{sy}} & \mathbf{x_{sz}} & \mathbf{0} \\ 0 & 0 & 0 & 1 \end{bmatrix}, \tag{3.6}$$

where $\mathbf{x_{sz}} = \mathbf{m_s}$, $\mathbf{x_{sx}} = \begin{bmatrix} 0 \\ 0 \\ -1 \end{bmatrix} \times \mathbf{x_{sx}}$ and $\mathbf{x_{sy}} = \mathbf{x_{sx}} \times \mathbf{x_{sz}}$.

Afterwards, we can project points on the viewing sphere to the catadioptric image plane by forward equation. Because the intensity of pixel on virtual perspective image equals to the intensity of its corresponding point on catadioptric image plane, we can assign the intensity of perspective image. For the smoothness of virtual perspective image, the intensity

of each pixel will be calculated by bilinear interpolation [47]. Finally, we can get virtual perspective image which we want to observe. Furthermore, we can pan, tilt and zoom the virtual perspective camera by changing the point of interest and the virtual perspective camera parameters.

3.3 Optimization of Viewing Sphere Model Parameters

In previous section, we estimate the initial parameters of viewing sphere model. In many aspects, the error of initial parameters may be introduced like the error of perspective camera parameters, the mirror is not a perfect hyperboloid or the error of central catadioptric camera installation. Therefore, we will refine the parameters of viewing sphere model in this section.

We have already estimated the initial parameters of viewing sphere model, and can calculate virtual perspective image of central catadioptric image in the last section. If the parameters of viewing sphere model is correct, the perspective image should be like reality. Otherwise, the constructed perspective image is distorted. The concept of the proposed method is to find the parameters which can generate virtual perspective image which is like the reality most. In our method, we use a planar pattern to estimate the measurement of the correctness of viewing sphere model parameters (figure 3.4).

We introduce an optimization procedure to refine the parameters of VSM. In the optimization procedure, we calculate virtual perspective image of the planar pattern first. After that, we extract the feature points in virtual perspective image by following image processing techniques : image binarization, blob analysis and centroid estimation. Using the estimated feature points and their corresponding feature points on the planar pattern, we can estimate the relative position between the planar pattern and the image plane by Zhang's method (figure 3.5). In Zhang's method, he calibrates the perspective camera by using the 3D points and their corresponding 2D image points. The image formation equation is as following:

$$\lambda\tilde{\mathbf{x}} = \mathbf{K}[\mathbf{R}|\mathbf{t}]\tilde{\mathbf{M}}, \tag{3.7}$$

where $\tilde{\mathbf{x}}$ is the augmented vector of image point; $\tilde{\mathbf{M}}$ is the augmented vector of 3D point; $\mathbf{K}$

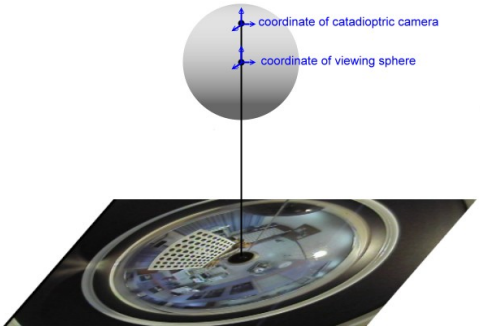

(a) Original image

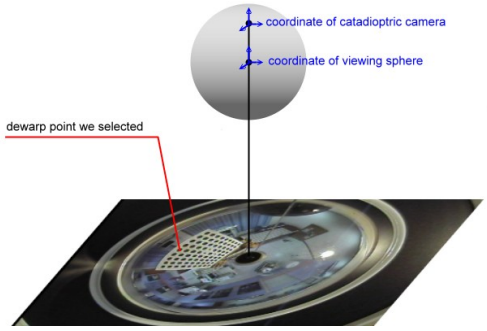

(b) Selecting a unwarping point

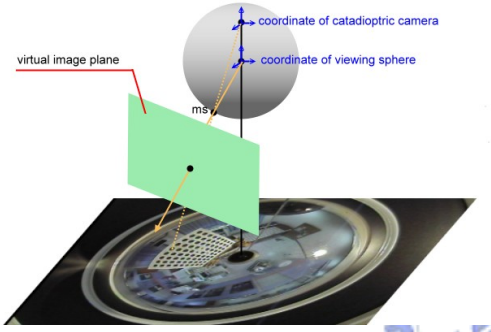

(c) Setting the virtual image plane

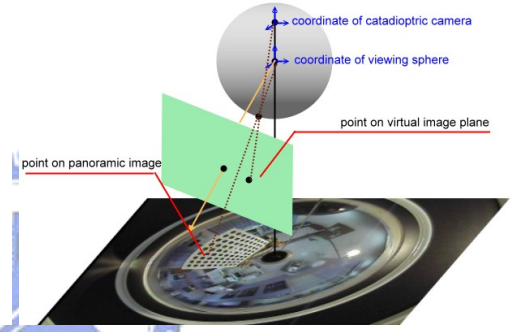

(d) Calculating the intensity

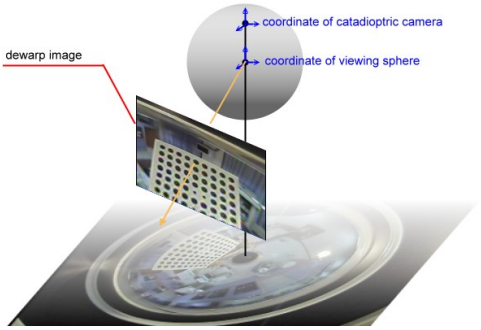

(e) Virtual perspective image

Figure 3.3: **Virtual perspective image construction from original catadioptric image.** The first image is original image of catadioptric camera (figure a). At first, we select a point of interest from original catadioptric image and calculate the corresponding 3-D light ray by backward equation (figure b). Next, we set the intrinsic parameters of the virtual perspective camera and then we have the virtual image plane (figure c). For every pixel on the virtual image plane, we calculate the corresponding point on catadioptric image by forward equation (figure d). Finally, we get virtual perspective image which we want to observe (figure e). Furthermore, we can pan, tilt and zoom the virtual perspective camera by changing the point of interest and the virtual perspective camera parameters.

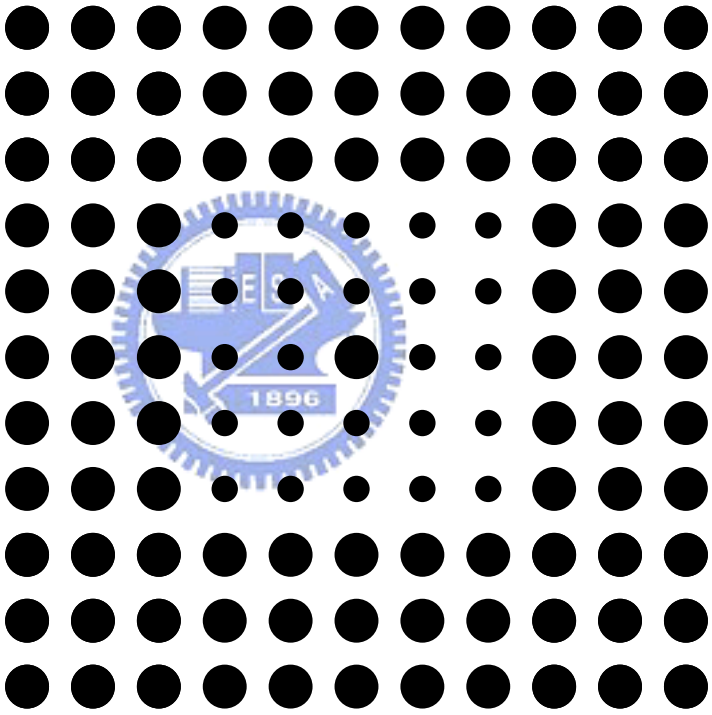

Figure 3.4: **The planar calibration pattern for optimization procedure.** The planar pattern is designed using language *PostScript*. There are 121 (11×11) feature points on the planar pattern. The diameter of big circle is $1cm$, the diameter of small one is $0.6cm$, and the distance between each feature point is $1.5cm$. Because of the special arrangement of big circle and small circle, we can estimate the middle feature point conveniently.

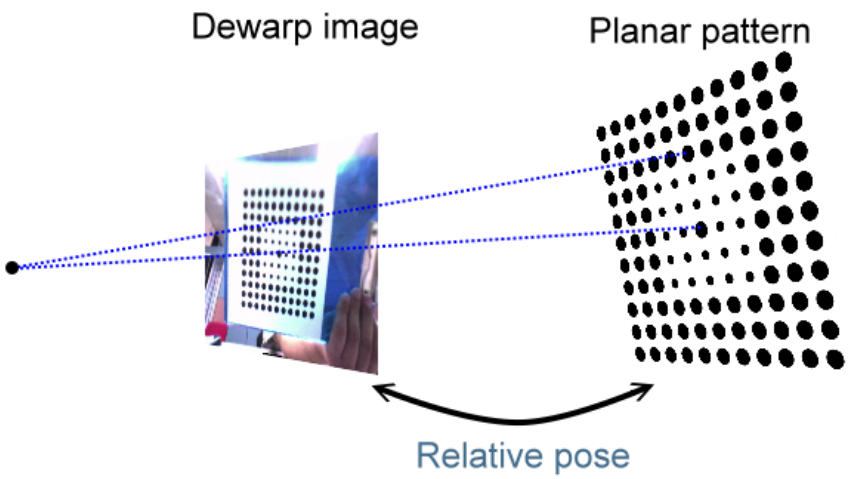

Figure 3.5: **Relative pose between planar pattern and virtual perspective image.**

is the intrinsic parameters of perspective camera; and $[\mathbf{R}|\mathbf{t}]$ is the extrinsic parameters of the perspective camera. In Zhang's case, he estimates the homography between 3D points and corresponding image points first. Then, he decomposes the homography matrix into two matrix, intrinsic and extrinsic matrix. In our case, we only have to estimate the extrinsic parameters, i.e. the relative pose, and the intrinsic parameters of the virtual perspective camera is known in advance. Therefore, we can estimate the relative position between the planar pattern and the image plane by Zhang's method using one image of the calibration pattern.

After the estimation of relative pose, we project the feature points on the planar pattern into virtual perspective image plane by using the transformation matrix we estimated. We calculate the distance between the extracted feature points on virtual perspective image and the feature points projected from the planar pattern, called reprojection error (figure 3.6). By the reprojection error, we can measure the correctness of virtual perspective image and the parameters of viewing sphere model.

To refine the parameters of viewing sphere, we can minimize the reprojection error by

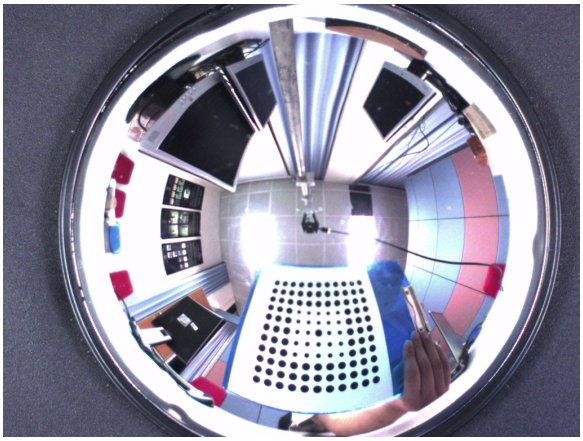

(a)

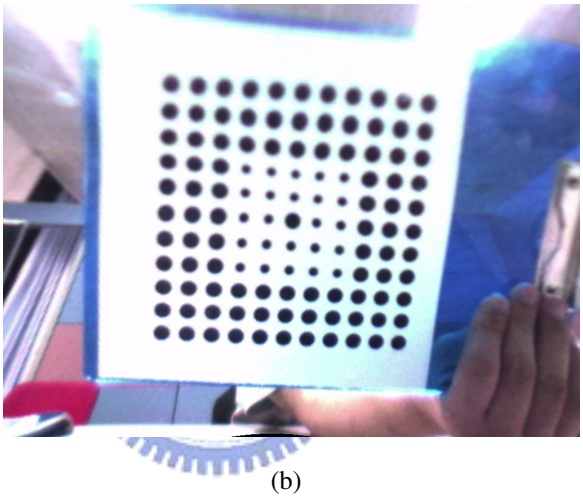

(b)

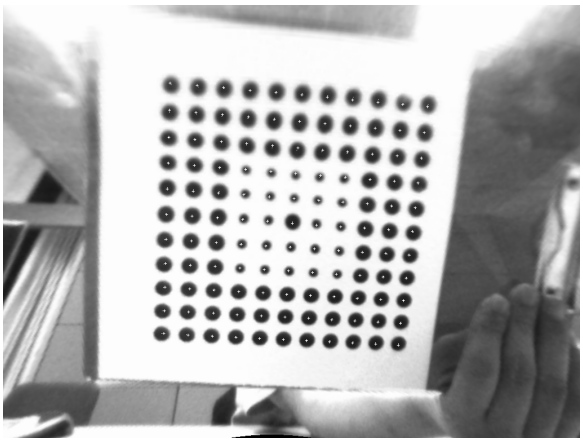

(c)

Figure 3.6: **Virtual perspective image and the reprojection error of feature points.** The top figure is the original image of central catadioptric camera (figure a). The middle image is virtual perspective image we calculated using the initial parameters of viewing sphere model (figure b). In the bottom image, the dot mark is the feature points of virtual perspective image and the cross mark is the points projected from the planar pattern (figure c). The distance between the dot mark and the cross mark is the reprojection error of the feature point.

minimizing the objective function :

$$\sum_{i=1}^{n}\sum_{j=1}^{m}\|F(\mathbf{m_{ij}}) - F(\hat{m}(\mathbf{A}, \mathbf{R_i}, \mathbf{t_i}, \mathbf{M_j}))\|, \tag{3.8}$$

where function $F()$ performs a mapping from the point on virtual perspective image plane to its corresponding point on catadioptric image plane, and function $\hat{m}()$ performs a mapping from the point on planar pattern to its corresponding point on virtual perspective image plane. Using the above objective function, we transform the points on virtual perspective image plane to points on catadioptric image plane and then calculate the reprojection error. The reason why we calculate the reprojection error after the transformation is that viewing sphere parameter f_e influences the size of planar pattern in virtual perspective image. If we do not apply the transformation before we calculate the reprojection error, the result of the optimization will be incorrect and bias to large value of f_e. Therefore, we need to apply the transformation before calculate the reprojection error.

For better accuracy of camera calibration, the calibration patterns had better be distributed all over the image and the number of the calibration patterns appearing in the image should be as many as possible. Hence, we take images of planar pattern for seven times (the more the better) in different directions. Then, we estimate the relative pose between each virtual camera and its corresponding planar pattern.

In the following, we show that moving a calibration plate around the catadioptric camera is equivalent to placing the same calibration plate at different poses relative to a static, virtual, perspective camera (figure 3.7). We can then use this set of unwarped perspective images to calculate the relative poses of the calibration plate as well as the projection error of the feature points on the calibration plate by using the homography method. In Zhang's calibration method, he considers the perspective camera does not move and the planar pattern moves randomly. The extrinsic parameters can be estimated by using his decomposition algorithm. In our method, although the virtual camera moves, we also consider the camera does not move and the planar pattern moves randomly. Hence, we can also get the relative pose between each virtual camera and its corresponding planar pattern by Zhang's method.

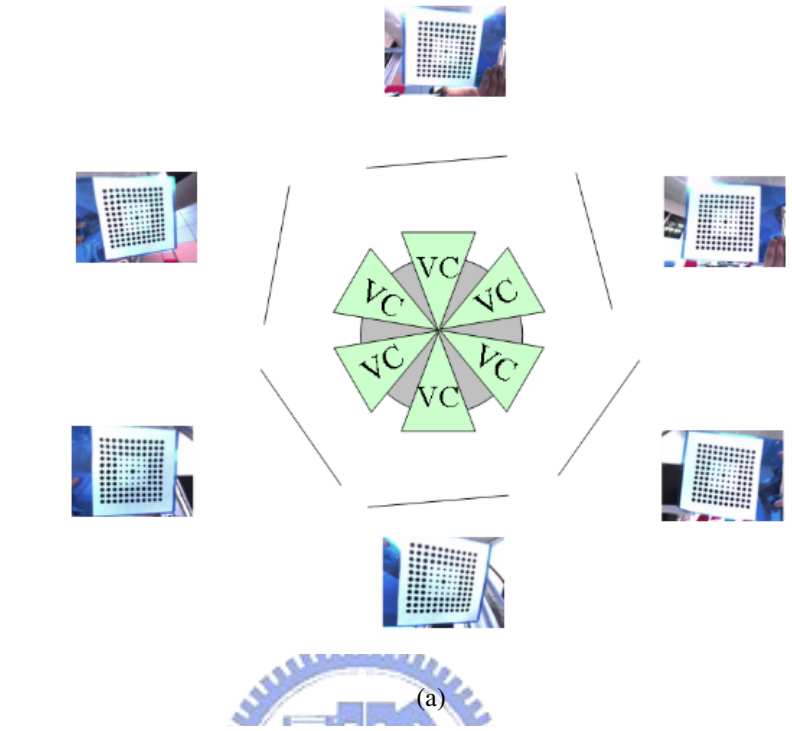

(a)

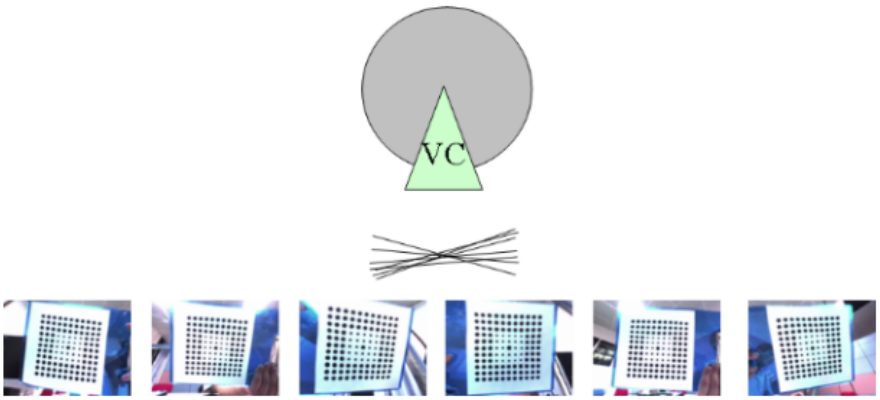

(b)

Figure 3.7: Relative position estimation using Zhang's method.

3.4 Summary

At last, we summarize the calibration procedure for central catadioptric camera. In the beginning, we have the original image of central catadioptric camera. Using the initial parameters of viewing sphere, we can calculate virtual perspective image of planar pattern from original central catadioptric image. Next, we estimate the relative pose between the image plane and planar pattern by homography. Then, we calculate the reprojection error of virtual perspective image. According to the reprojection error, we can measure the accuracy of the viewing sphere model. Finally, we will get the optimal viewing sphere model parameters through the iterative optimization procedure until the reprojection error is minimized.

The recommended calibration procedure for central catadioptric camera is as follows:

1 Print the calibration pattern and attach it on a reasonable planar plate.

2 Place the planar calibration plate several times surrounding the camera and capture an image for each pose of the calibration plate.

3 Detect feature points on the images.

4 Estimate the initial parameters of the viewing sphere model.

5 Refine all parameters by proposed optimization procedure.

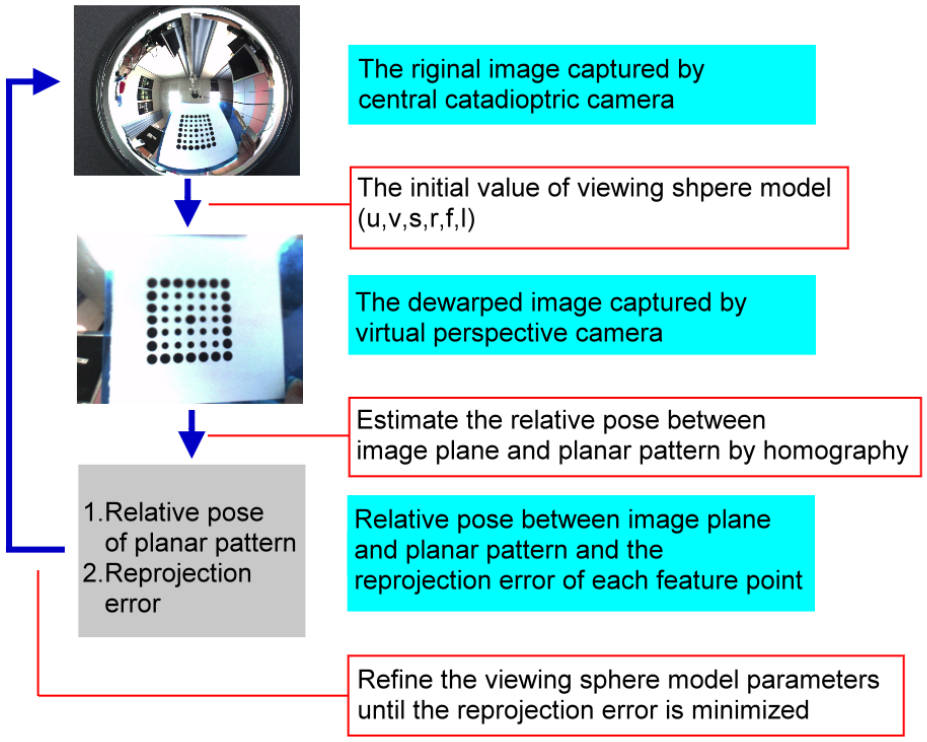

Figure 3.8: **Optimization procedure for viewing sphere model parameters.** In the beginning, we have the original image of central catadioptric camera. Using the initial parameters of viewing sphere, we can calculate virtual perspective image of planar pattern from original central catadioptric image. Next, we estimate the relative pose between the image plane and planar pattern by homography. Then, we calculate the reprojection error of virtual perspective image. According to the reprojection error, we can measure the accuracy of the viewing sphere model. We will optimize the viewing sphere model parameters until the reprojection error is minimized.

Chapter 4

Non-central Catadioptric Camera Calibration using LCDs

In this chapter, we introduce the proposed calibration method for non-central catadioptric camera using planar calibration objects, LCD. First, we measure the 3D position of feature points on LCD by a calibrated central catadioptric camera. Afterwards, we introduce a general image formation model for non-central catadioptric camera, the reflected ray model (RRM). At last, we introduce an initial estimation for the mirror posture proposed by Mashita, and an optimization method for refining the parameters of non-central catadioptric camera by minimizing the calibration error.

4.1 3D Corresponding Points Estimation

In this section, we introduce proposed 3D corresponding points estimation method for non-central catadioptric camera. In classical photogrammetric calibration methods, there are two problems we must solve before calibrating the camera. First, it requires an expensive calibration apparatus and an elaborate setup to obtain accurate 3D position in 3D space. Besides, the correspondence between 2D image points and 3D world points is given manually. In our proposed method, we solve the two problems by using a calibrated central catadioptric camera and LCD. At first, we estimate 3D position of feature points on LCD by a calibrated central catadioptric camera. Next, we remove the central catadioptric camera and place the non-central catadioptric camera in the same place. We can assume the relative position between the LCD and the mirrors of central and non-central catadioptric camera is the same. Then, the correspondences between 2D image points and 3D world points are given automatically by the bite codes generated by LCD.

Relative pose between LCD and mirror

In this section, we estimate 3D position of feature points on LCD by using a calibrated central catadioptric camera. The relative pose between LCD and mirror can be described in two transformations, *rotation of virtual perspective camera* and *relative pose between virtual perspective camera and LCD* (figure 4.1).

The calculation of the rotation matrix of virtual perspective camera is the same with the one in chapter 3. Given a unwarping point $\mathbf{m_0}$, we can calculate its corresponding 3D light

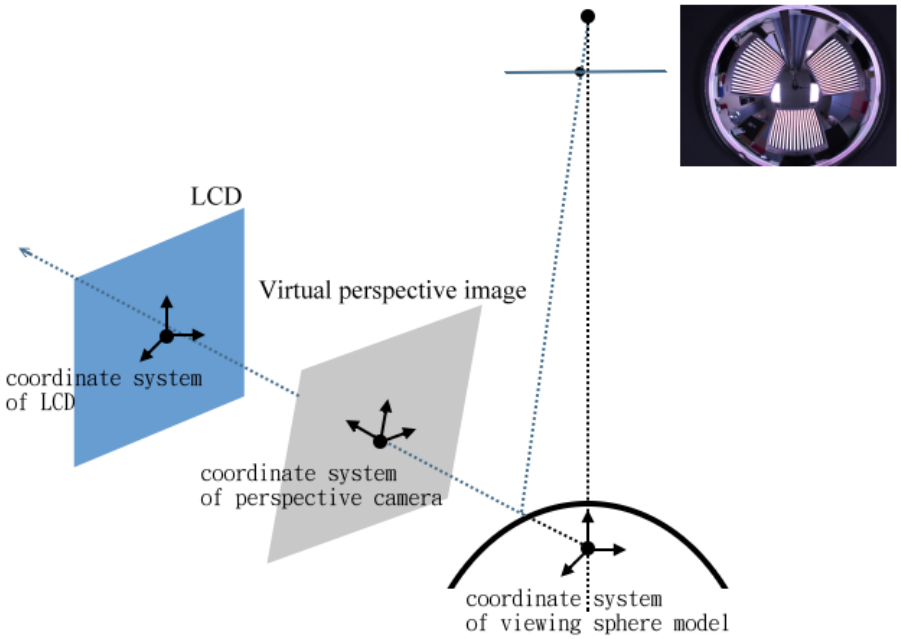

Figure 4.1: **Relative pose between the LCD and the mirror.** The relative pose between LCD and mirror can be described in two transformations, rotation of virtual perspective camera and relative pose between virtual perspective camera and LCD. We can estimate the two matrix by a calibrated central catadioptric camera.

ray, $\mathbf{m_s} = (\mathbf{x_s}, \mathbf{y_s}, \mathbf{z_s})$,using parameters of VSM.

$$\begin{cases} x_s = \lambda x' \\ y_s = \lambda y' \\ z_s = \lambda - l \\ \lambda = \frac{l+\sqrt{x'^2(1-l^2)+y'^2(1-l^2)+1}}{x'^2+y'^2+1} \end{cases} \tag{4.1}$$

Then, the rotation matrix ${}^{cata}\mathbf{R}_{pers}$ is as following.

$${}^{mirror}\mathbf{R}_{pers} = \begin{bmatrix} \mathbf{x_{sx}} & \mathbf{x_{sy}} & \mathbf{x_{sz}} \end{bmatrix} \begin{cases} \mathbf{x_{sz}} = \mathbf{m_s} \\ \mathbf{x_{sx}} = \mathbf{z} \times \mathbf{x_{sx}} \\ \mathbf{x_{sy}} = \mathbf{x_{sx}} \times \mathbf{x_{sz}} \end{cases} \tag{4.2}$$

Afterwards, the relative pose between virtual perspective camera and LCD, ${}^{pers}\mathbf{R}_{LCD}$, is estimated by Zhang's method [50]. Using Zhang's method, we can estimate the relative pose between two planes. Therefore, we can obtain the relative pose between virtual perspective image and plane of LCD. After estimating the rotation matrix of virtual perspective camera and the relative pose between virtual perspective camera and LCD, we can transform feature points on LCD from original coordinate system of LCD to the one of mirror coordinate system.

Correspondence estimation

In the following, we introduce the automatic method for finding corresponding points we presented. At first, we mount the LCD which display 20 different patterns at a fixed location. Non-central and central catadioptric cameras which are located alternately in the same place capture the images of LCD. Because the LCD is located in a fixed location and non-central and central catadioptric cameras are also placed in the same position, two pixels of non-central and central catadioptric image which are projected by the same pixel of the LCD will project to the same 3D rays in the space. Then, we can estimate the corresponding points using the images of LCD in both catadioptric cameras (figure 4.2).

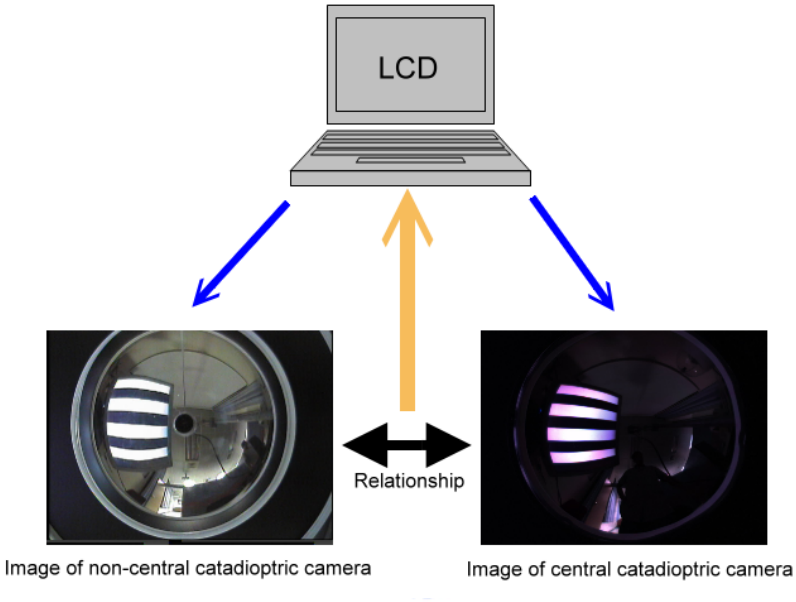

Figure 4.2: **Corresponding points estimation by bitcode generated by LCD.** Because the LCD is located in a fixed location, two pixels of non-central and central catadioptric camera which are projected by the same pixel of the LCD will project to the same 3-D rays in the space. Then, we can estimate the corresponding points using the LCD images of both catadioptric camera.

LCD pixel encoding

After the setting of LCD and camera, we need to encode every pixel on LCD a unique code to identify its position. For this purpose, there are 20 different images displayed on LCD sequentially. By displaying the patterns on LCD, we can identify the position of the pixel by the colors displayed by the pixel.

Using 20 different patterns shown by LCD, we can encode each pixel on the LCD an unique bit code (figure 4.3). These 20 images are all monochrome. Ten of them are alternating with black and white vertically and another ten of them are alternating horizontally. The first pattern of the ten images which are alternating vertically has two blocks, the left half block is black and the right half block is white. Using this pattern, we can distinguish whether one pixel is in the left block or in the right block by the color of the pixel. The second pattern has four blocks, the color sequence is black, white, black and white. Using the first pattern and this pattern, we can we can distinguish one pixel is in which block of the four blocks. And so on, we can know the horizontal position of every pixel using these 10 patterns. In the same way, we can know the vertical position of every pixel by using these 10 patterns which alternates horizontally. Eventually, we can know the exact position of every pixel on LCD using these 20 patterns.

After displaying these 20 patterns sequentially, each pixel on the LCD can generate a 20 bits code by determining which color is shown by the pixel when displaying the patterns. The resolution of the LCD we used is 1024×768, among 2^{19} and 2^{20}. The code with 20 bits can represent 2^{20} numbers. Because, the number of pixels on LCD is smaller than the number which the pattern can generate, and the code generated by the patterns we designed is different pixel by pixel. Hence, the code of each pixel is unique.

Image process of corresponding points estimation

After introducing the encoding of pixels on LCD, we extract the feature points from central and non-central catadioptric images. We need to process 20 central catadioptric images and 20 non-central catadioptric images and the processes are described in the following.

I. Cropping LCD part in the image Because we only have to process the area of image

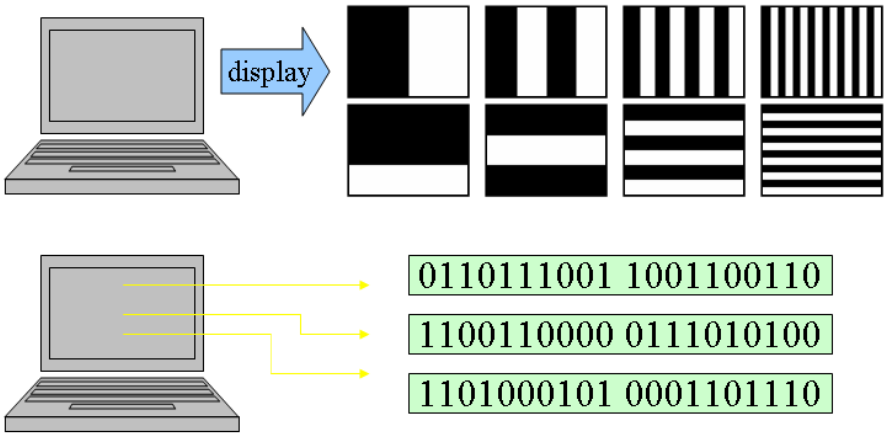

Figure 4.3: **The encoding of pixels on the LCD.** After LCD displays these 20 patterns sequentially, each pixel on LCD can generate a 20 bits code by determining which color is shown by the pixel when displaying the patterns. And the code of each pixel is unique.

which LCD appears, we segment the image at first (figure 4.4(a)). This process can also improve the result of binarization without the influence generated by other areas in the image.

II. Binarization We binarize the image of LCD by Otsu's method (figure 4.4(a)). Using Otsu's method, we can get a value of threshold. When intensity of the pixel is higher than the threshold, intensity of the pixel will update to 255. Otherwise, intensity of the pixel will update to 0.

III. Bitcode generation In this step, we encode every pixel on LCD by a binary bitcode which length is 8. The reason why we do not use entire 20 images is the problem of aliasing, i.e. the resolution of real LCD is much bigger than the resolution of the image of LCD. Therefore, we only use 8 bits to encode every pixel in LCD image.

IV. Pixel Grouping After above steps, every pixel in LCD image has its own bitcode. But the bitcode of each pixel is not unique because we only use 8 images of all. Next, we group pixels with the same bitcode into the same image (figure 4.4(b)). Thus, there

will be 192 ($2^8 \times \frac{3}{4}$) images for maximum after classification.

V. Connective component analysis Due to the problem of aliasing, there will be some pixels which its bitcode is not correct. These pixel will not be connected with the pixels which its bitcode is correct. To solve this problem, we eliminate these pixels by connective component analysis (figure 4.4(c)). After the process of connective component analysis, we can obtain many connective components. We only keep the biggest connective component and discard the others component because we consider they are noise.

VI. Area fraction filter Besides the above process, we also eliminate the images which the biggest connective component is too small (figure 4.4(c)), because we do not know the biggest component whether it is a correct blob or it is not.

After the above process for central and non-central catadioptric images, we can obtain the feature points in non-central and central catadioptric images. The coordinate of the feature point is the mass center of the block assembled by pixels with the same bitcode. The reason why we group the pixels with the same code into a block is to increase the accuracy of the pixel position. If we only use a pixel to generate a feature points, the accuracy of position of pixel will decrease largely due to the phenomenon of aliasing.

At last, we can estimate the corresponding points by matching the bitcode of the feature points, because the same bitcode will map to the same position on LCD. For instance in figure 4.5, the bitcode of the pixel on the left top position of LCD is ”11111101”. The feature points which the bitcode both are ”11111101” in the non-central and central catadioptric images are a pair of corresponding points, because they are both projected by the same pixel on the LCD.

4.2 Image Formation Model for Non-central Catadioptric Camera

In chapter 2, we introduce two image formation models for non-central catadioptric camera, **Reflected Ray Model** and **Caustic Model**. For the application of calibration, we

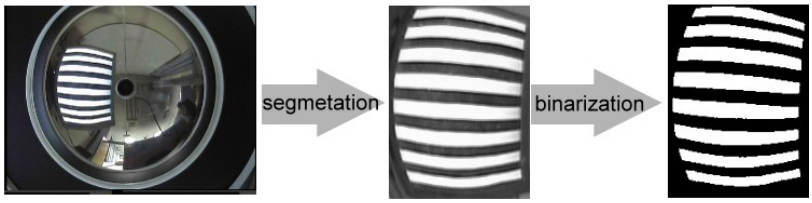

(a)

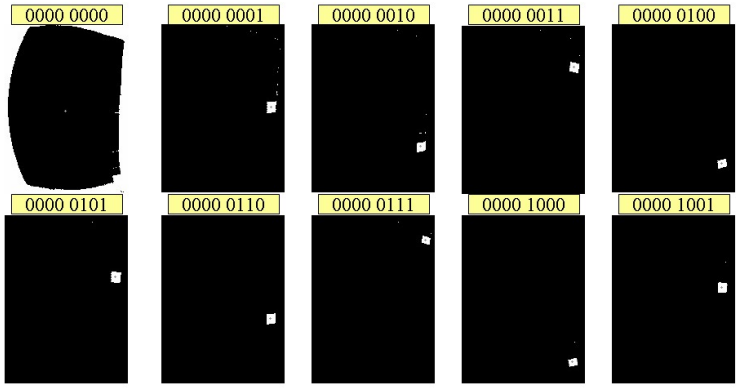

(b)

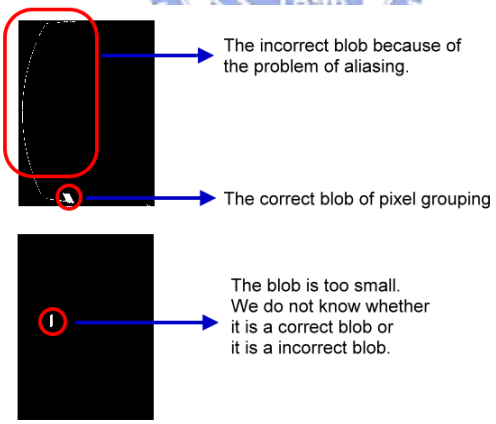

(c)

Figure 4.4: **Image processes for feature extraction.** (a) is the preprocess of feature extraction. Because we only have to process the area of image which LCD appears, we segment the image at first. After that, we binarize the image of LCD by Otsu's method. In subfigure (b), we group pixels with the same bitcode into the same image. In subfigure (c), we eliminate the wrong connective components and wrong images. After the above process, we can obtain the coordinate of every feature point.

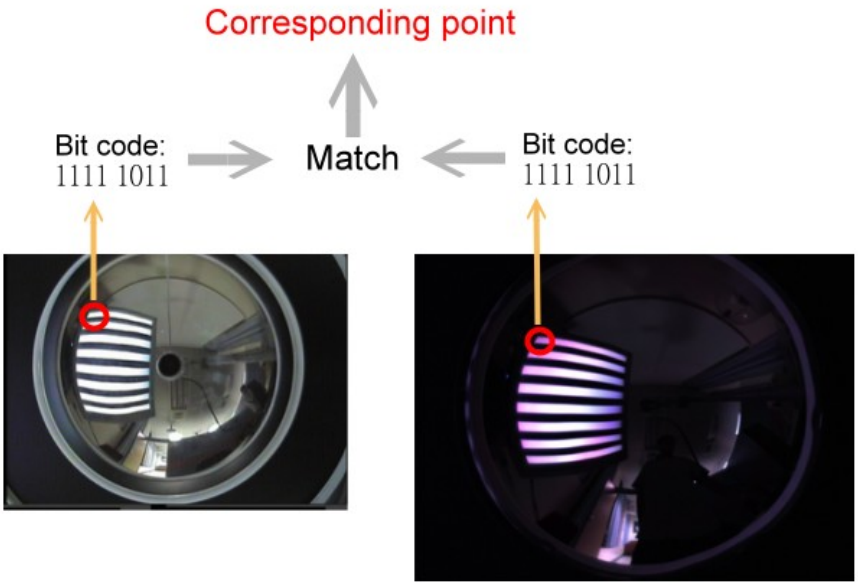

Figure 4.5: **Corresponding point estimation by bitcode matching.** For instance, the bitcode of the pixel on the left top position of LCD is ”11111101”. The feature points which the bitcode both are ”11111101” in the non-central and central catadioptric image are a pair corresponding points, because they are both projected by the same pixel on the LCD.

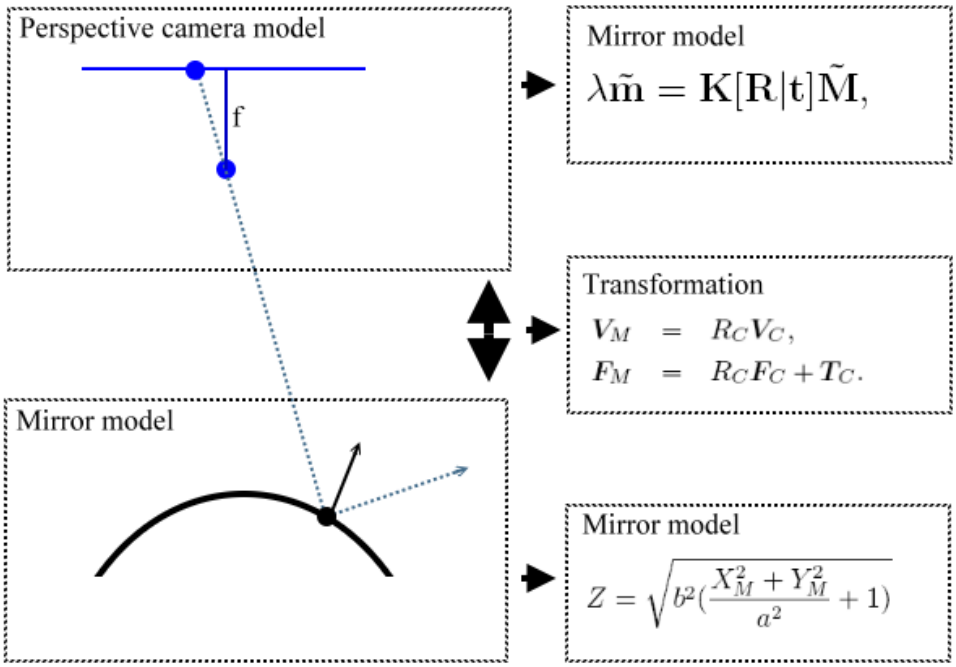

Figure 4.6: **Reflected ray model.**

only need to obtain the geometrical information, thus, we choose the reflected ray model as our image formation model for non-central catadioptric camera.

For central catadioptric cameras, the relative position between the camera and the mirror is fixed. But for non-central catadioptric camera, the relative position between the camera and the mirror is arbitrary. To estimate the relative pose between the camera and the mirror, the reflected ray model separates the image formation model into *perspective camera model* and *mirror model*. There is a transformation to relate the coordinate system between camera and mirror (figure 4.6).

perspective camera model The perspective camera model is the pinhole model introduced in chapter 2. Give a world point $\mathbf{M}$ based on arbitrary camera coordinate system and its corresponding image point $\mathbf{m}$. The relationship of image point $\mathbf{m}$ and $\mathbf{M}$ is given by

$$\lambda\tilde{\mathbf{m}} = \mathbf{K}\tilde{\mathbf{M}}, \quad \textbf{with} \quad \mathbf{K} = \begin{bmatrix} \alpha & \gamma & u_0 \\ 0 & \beta & v_0 \\ 0 & 0 & 1 \end{bmatrix} \tag{4.3}$$

Transformation Transformation between the camera and the mirror can be described by a rotation matrix $\mathbf{R_C}$ and a translation vector $\mathbf{T_C}$. A ray from the camera in the camera coordinate, $\mathbf{V_C}$, and a point in the camera coordinate, $\mathbf{P_C}$, are transformed to the mirror coordinate system by using rotation matrix $\mathbf{R_C}$ and translation vector $\mathbf{T_C}$ as follows:

$$V_M = R_C V_C, \tag{4.4}$$

$$P_M = R_C P_C + T_C. \tag{4.5}$$

Mirror model There are many mirror types which can be applied in non-central catadioptric camera, such as parabolic, hyperbolic, spherical and elliptical mirror. We just introduce hyperbolic mirror for instance. A point $\mathbf{P} = (\mathbf{x_M}, \mathbf{y_M}, \mathbf{z_M})$ on the hyperbolic mirror can be described as the following equation,

$$\frac{x_M^2 + y_M^2}{a^2} + \frac{z_M^2}{b^2} = -1, \tag{4.6}$$

where a and b are parameters of the hyperbolic mirror. The distance between two focus $2c$ is $2\sqrt{a^2 + b^2}$ and the eccentricity of the hyperbolic ε is $\sqrt{1 + \frac{b^2}{a^2}}$.

4.3 Parameters estimation of Reflected Ray Model

In this section, we estimate camera parameters of non-central catadioptric camera using 2D and 3D correspondence estimated in the first section. At first, we estimate an initial value for the reflected model using parameter of perspective camera and the mirror. Then, we refine the parameters of reflected model by minimizing the distance between the light ray calculated from image point and the 3D point estimated by the calibrated central catadioptric camera.

Initial estimation of reflected ray model

In reflected ray model, we can estimate the parameters of perspective camera and hyperbolic mirror in advance. Hence, we can calibrate the perspective camera by Zhang's method [50] and obtain the mirror parameter by the specification before we calibrate non-central catadioptric camera. What we only need is to estimate the relative pose between perspective camera and mirror, i.e. $\mathbf{R_C}$ and $\mathbf{T_C}$. We have two options for initial parameters of the relative pose according to the non-central catadioptric camera. If the misalignment of mirror is minor, we can set initial mirror pose as central one, i.e. $\mathbf{R_C} = \mathbf{I}$ and $\mathbf{T_C} = (\mathbf{0}, \mathbf{0}, \mathbf{c})$, where c is the distance between one focus to the center of the hyperbola. If the misalignment is serious, we can estimate the initial value by Mashita's method which uses mirror boundary to estimate the relative pose [48].

Optimization of reflected ray model

After the initial estimation of parameters in reflected ray model, we refine the parameter by minimizing the distance between light ray calculated by an image point and its corresponding 3D world point (figure 4.7).

Given a world point $\mathbf{P} = (\mathbf{p_x}, \mathbf{p_y}, \mathbf{p_z})$ and its corresponding image point $\mathbf{p}$, we can calculate the projected light ray by initial camera parameters. The projected light ray includes two component, the coordinate of reflected point on mirror $\mathbf{M} = (\mathbf{m_x}, \mathbf{m_y}, \mathbf{m_z})$ and the vector of reflective light ray $\mathbf{V} = (\mathbf{v_x}, \mathbf{v_y}, \mathbf{v_z})$. Hence, we can represent the reflected light ray by $\mathbf{M}+\mathbf{kV}$, where k is a arbitrary scale. Next, we calculate the distance between world point $\mathbf{P}$ and the reflected light ray. We can solve k by following equation.

$$(\mathbf{V}, \mathbf{M} + \mathbf{kV} - \mathbf{P}) = \mathbf{0} \tag{4.7}$$

$$k = \frac{(w_x - m_x)v_x + (w_y - m_y)v_y + (w_z - m_z)v_z)}{v_x^2 + v_y^2 + v_z^2} \tag{4.8}$$

After solving the scale k, we can obtain the nearest point on the light ray with world point $\mathbf{P}$. Then, the distance between the two points is the calibration error. The objective function of the optimization for non-central catadioptric camera is as following.

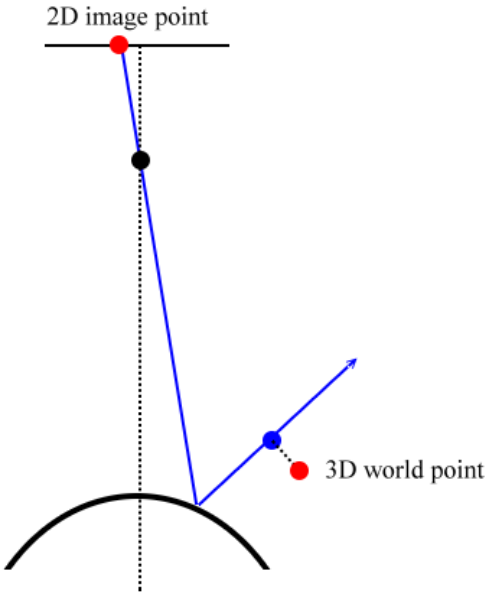

Figure 4.7: **Calibration error of estimated parameters in reflected ray model.** The calibration error is the distance between light ray calculated by an image point and its corresponding 3D world point.

$$\sum_{i=1}^{n}\sum_{j=1}^{m}\|\mathbf{P_{ij}} - \hat{\mathbf{m}}(\mathbf{R_C}, \mathbf{T_C}, \mathbf{p_{ij}})\|, \tag{4.9}$$

where index i is the number of LCD, and index j is the number of feature points on LCD, $\mathbf{P_{ij}}$ is the feature point on LCD which coordinate is estimated by a calibrated central catadioptric camera, $\mathbf{p_{ij}}$ is the extracted image point on non-central catadioptric image plane and $[\mathbf{R_C}|\mathbf{T_C}]$ is the mirror pose. By minimizing the above objective function, we can obtain accurate relative pose between the coordinate system of mirror and the one of LCD.

4.4 Summary

At last, we summarize the calibration procedure for non-central catadioptric camera. In the beginning, we estimate the 3-D coordinate of feature points on LCD by a calibrated central catadioptric camera. Next, we replace the central catadioptric camera with a non-central catadioptric camera in the same place. After obtaining the correspondence of non-central catadioptric camera, we can get the optimal reflected ray model parameters through the iterative optimization procedure until the reprojection error is minimized.

The recommended calibration procedure for non-central catadioptric camera is as follows:

1 Setup the LCDs at proper fixed positions (figure 4.9).

2 Detect the feature points on LCD on the central catadioptric image.

3 Estimate the 3D position of each feature point on LCD by a calibrated central catadioptric camera.

4 Replace the central catadioptric camera with a non-central catadioptric camera.

5 Detect the feature points on LCD on the non-central catadioptric image.

6 Estimate the initial parameters of the reflected ray model.

7 Refine all parameters by proposed optimization procedure.

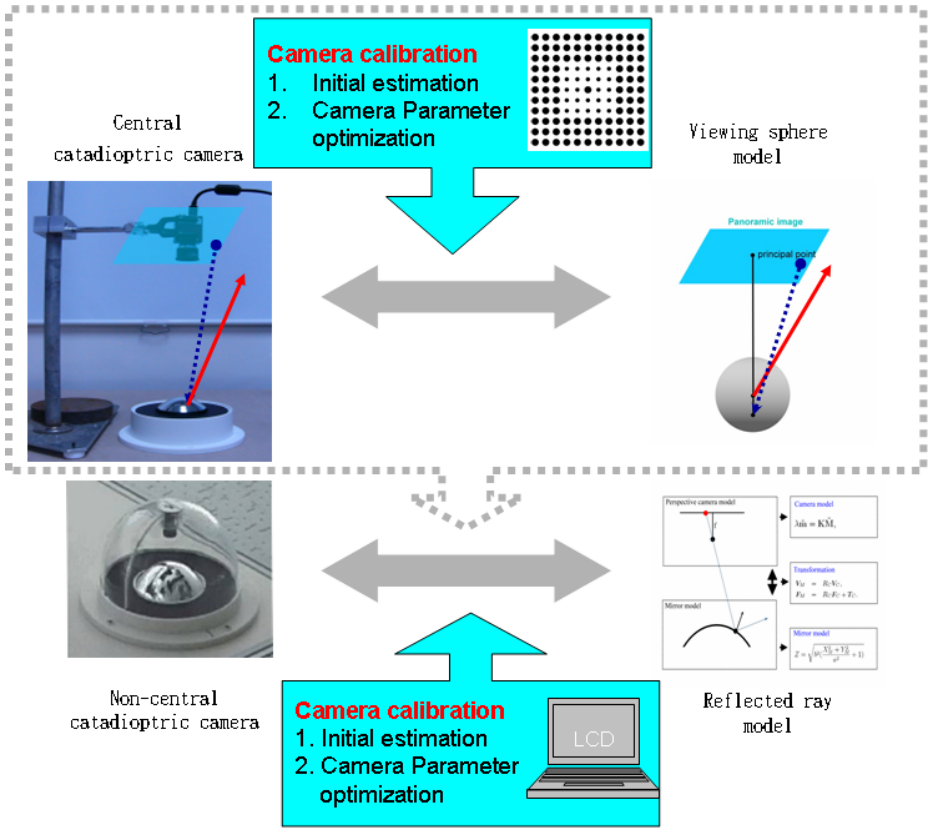

Figure 4.8: **Calibration procedure for non-central catadioptric camera calibration.**

Figure 4.9: **Setup of the LCD for non-central catadioptric camera calibration.**

Chapter 5

Experiment Results

For demonstration and verification, we implement our proposed calibration methods for central and non-central catadioptric camera. The procedures are implemented in C/C++ language, compiled by Microsoft Visual C++ 6.0 compiler [11] and executable on MS-WIN32 platform. We evaluate the performance of proposed methods by simulation data and real experiment. In simulation, the computer generates the simulation data of central catadioptric camera by viewing sphere model and the simulation data of non-central catadioptric camera by reflected ray model. In the real experiments, the central catadioptric camera is combined by a perspective camera (Marlin F-080C) and the same specification of mirror as the non-central catadioptric camera, and we use the MAPCAM made by the company EERISE as our non-central catadioptric camera.

In the first section, we evaluate the performance of the proposed calibration method for central catadioptric camera by simulation and real experiment. In the second section, we evaluate the performance of the proposed calibration method for non-central catadioptric camera. At last, we use the calibrated non-central catadioptric camera to navigate a mobile robot to demonstrate the performance of proposed calibration method.

5.1 Results of Central Catadioptric Camera Calibration

5.1.1 Simulation Experiment

In the simulation experiment, we can easily modify the parameters of the model and control the environment of the experiment. Using the simulation data, we can also evaluate the performance of calibration methods by comparing the calibration results and the ground truth. Hence, we evaluate the performance of proposed method using the simulation data in the following.

The simulated central catadioptric camera has following parameters: $f_e = 330$, $s = 0$, $r = 1$, $l = 0.95$, $u_0 = 512$ and $v_0 = 384$. The resolution of the image is 1024×768. The generation procedure of simulation data are described in detail in appendix A. In the simulation data, gaussian noise with zero-mean and σ standard deviation is added to these image points. We vary the noise level σ from 0.0 to 2.0 pixels. For each noise level, we perform 100 independent trials. For better accuracy of camera calibration, the

Noise level	f_e (%)	θ (%)	r (%)	l (%)	u_0 (%)	v_0 (%)	Error(pixel)
0	0.005	0.000	0.000	0.000	0.000	0.000	0.003
0.4	0.088	0.000	0.002	0.004	0.042	0.027	0.684
0.8	0.330	0.000	0.028	0.052	0.005	0.010	0.967
1.2	0.645	0.004	0.043	0.114	0.153	0.075	1.189
1.6	1.053	0.059	0.021	0.181	0.305	0.270	1.341
2.0	1.351	0.022	0.006	0.195	0.515	0.330	1.520

Table 5.1: **Simulation result of central catadioptric camera calibration.**

calibration patterns had better be distributed all over the image and the number of the calibration patterns appearing in the image should be as many as possible. We generate seven calibration patterns and there are 121 feature points on each calibration patterns. The simulated images are shown in figure (5.1).

The calibration results of proposed method are shown in table 5.1. In this table, the skew factor s is replaced by θ which is the angle between the two image coordinate axes. The relative error of the effective focal length is $(f_e - f_e^*)/f_e$ where f_e is the ground truth and f_e^* is the mean of the calibration results, and the relative error of other parameters are defined in the same way. The results show that the recovered parameters are accurate because the relative errors for each parameter in VSM is very small. When we elevate the noise level, we can also obtain precise camera parameters. Hence, the results show that our calibration method is accurate and robust.

For the purpose of performance comparison, we also implement Ying's calibration method using geometric invariants. The condition of Ying's simulation experiment is the same with one of ours. The results are shown in table 5.2. The results show that our calibration result is better than Ying's calibration result when the noise level is lower than $\sigma = 0.4$, and the principal point estimated by our method is always better than Ying's. But, our calibration result is worse than Ying's when the noise level is higher than $\sigma = 0.4$. The reason will be explained in the section of discussions.

To evaluate the performance of proposed objective function, we change one parameter

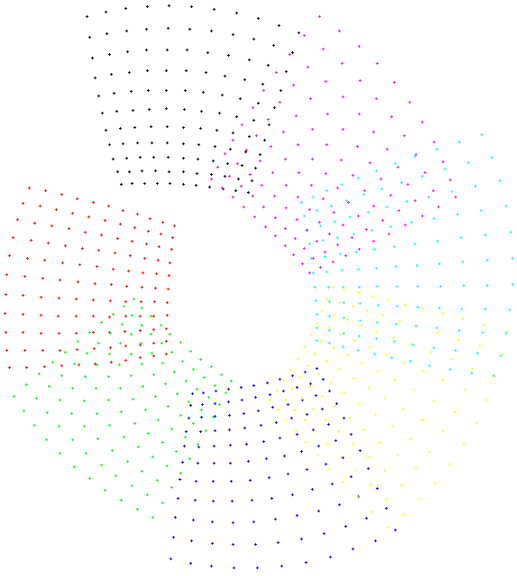

(a) Simulation data

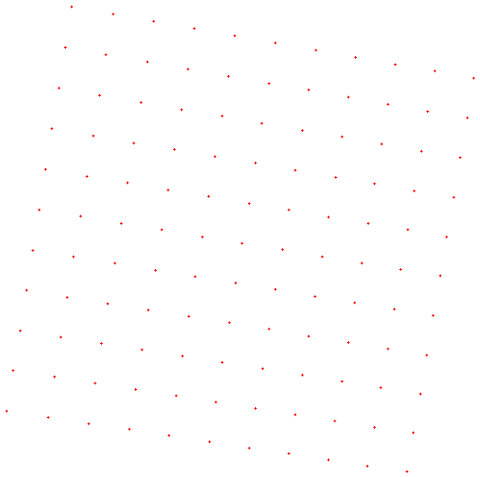

(b) Its virtual perspective image

Figure 5.1: **Simulation image contains seven calibration patterns and the virtual perspective image constructed using the ground truth.**

Noise level	f_e (%)	θ (%)	r (%)	u_0 (%)	v_0 (%)
0	4.242	0.042	0.024	0.252	1.574
0.4	0.691	0.025	0.003	0.225	1.951
0.8	0.015	0.026	0.016	0.508	1.359
1.2	1.292	0.037	0.013	0.176	1.073
1.6	0.909	0.017	0.029	0.833	0.845
2.0	0.584	0.000	0.022	0.797	0.488

Table 5.2: **Simulation result of Ying's method.**

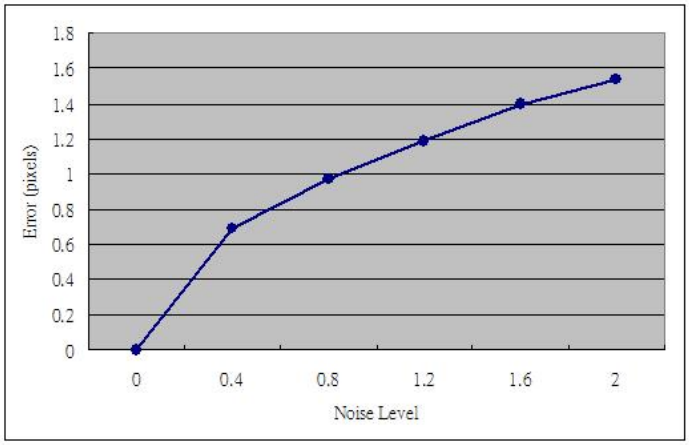

Figure 5.2: **Average estimation error of VSM parameters vs. the noise level of the image points.**

and fix other five parameters at one time to observe the influence of each parameter in VSM. The results are shown in figure 5.3. For each parameter, we calculate 200 sample points around the ground truth. It shows that there is a obvious gap for each parameter in VSM. For each parameter in VSM, the minimum of the objective function is located at the ground truth. Therefore, there is no chance for calibration result to trap in the local minimum. According to this experiment, it results show that our objective function is robust.

To evaluate the influence of the noise to the objective function, we add also gaussian noise with zero-mean and standard deviation ($\sigma = 1$) to the simulation data. The results are shown in figure 5.4. For each parameter in VSM, the minimum of the objective function is also located at the ground truth. Besides the skew factor l, the curve of the objective function is not stable while high noise level.

We also generate simulation data by the projection of a virtual calibration pattern in space to evaluate the performance of the feature extraction in our method. In the first simulation data, we obtain the feature points directly by reading text files, rather than several steps of image process. In this one, we extract the feature points by following techniques of image process, image binarization, blob analysis and centroid estimation. By comparing the results of two sets of simulation data, we can estimate the error generated during the process of feature extraction in image based simulation data.

In image based simulation data, we also generate seven calibration patterns by viewing sphere model and there are 121 feature points on each calibration patterns. The simulated images are shown in figure 5.5. For the verification of the performance of proposed objective function, we set several different initial parameters in this simulation experiment. The calibration results are shown in table 5.3. The simulation results show that the results estimated by our method can converge to the ground truth. The calibration results using the method presented by Ying [24] are shown in the same table for comparison. The results show that our method are still robust with bad initial estimation. Compared with Ying's method, the calibration results are not stable with bad initial estimation, especially for the parameter l. In the initial guess 4 ($f_e = 430$, $l = 0.850$), the result of Ying's method is far from the ground truth, but the result of our method is very close to the ground truth. Therefore, Ying assumes that the parameters l is known in advance in his calibration pro-

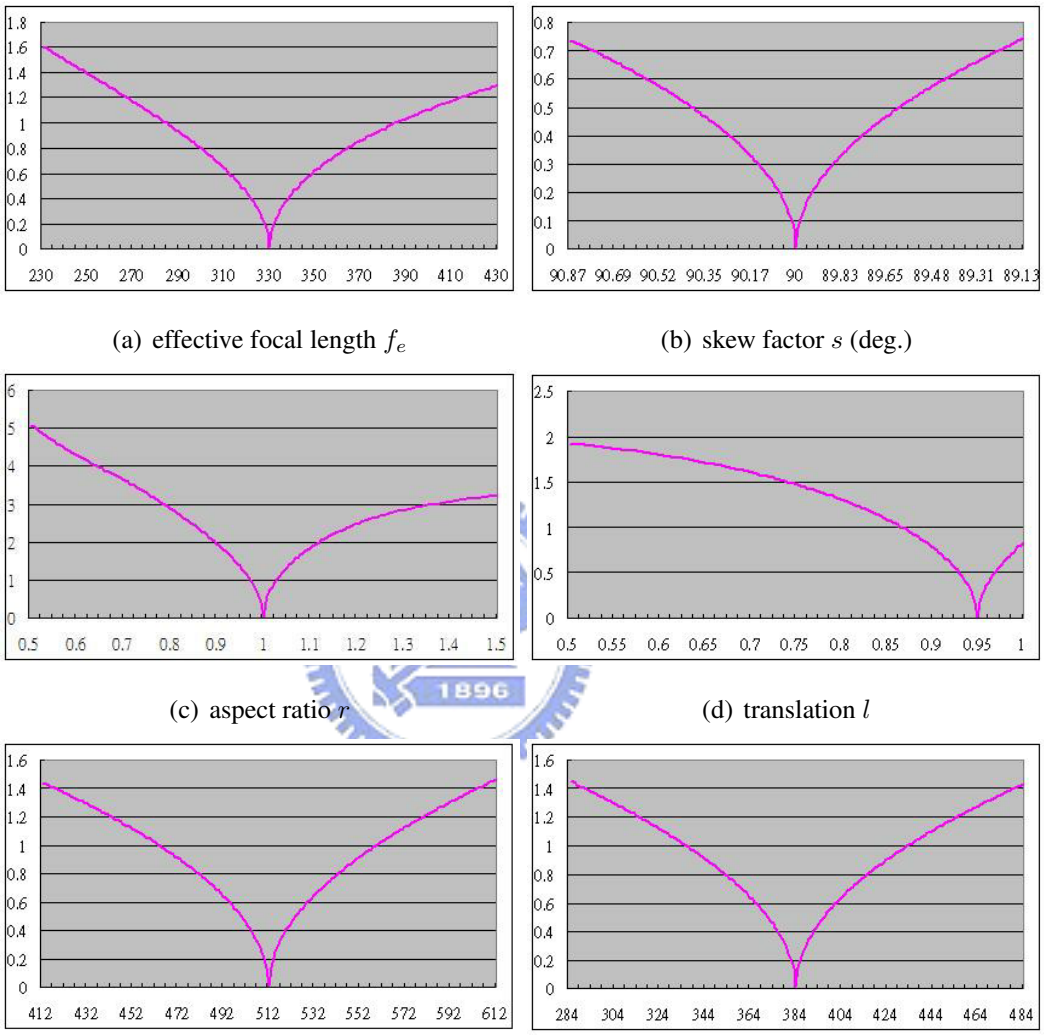

(a) effective focal length f_e (b) skew factor s (deg.)

(c) aspect ratio r (d) translation l

(e) principal point u_0 (pixel) (f) principal point v_0 (pixel)

Figure 5.3: **The influence of parameters in VSM to the objective function ($\sigma = 0$).**

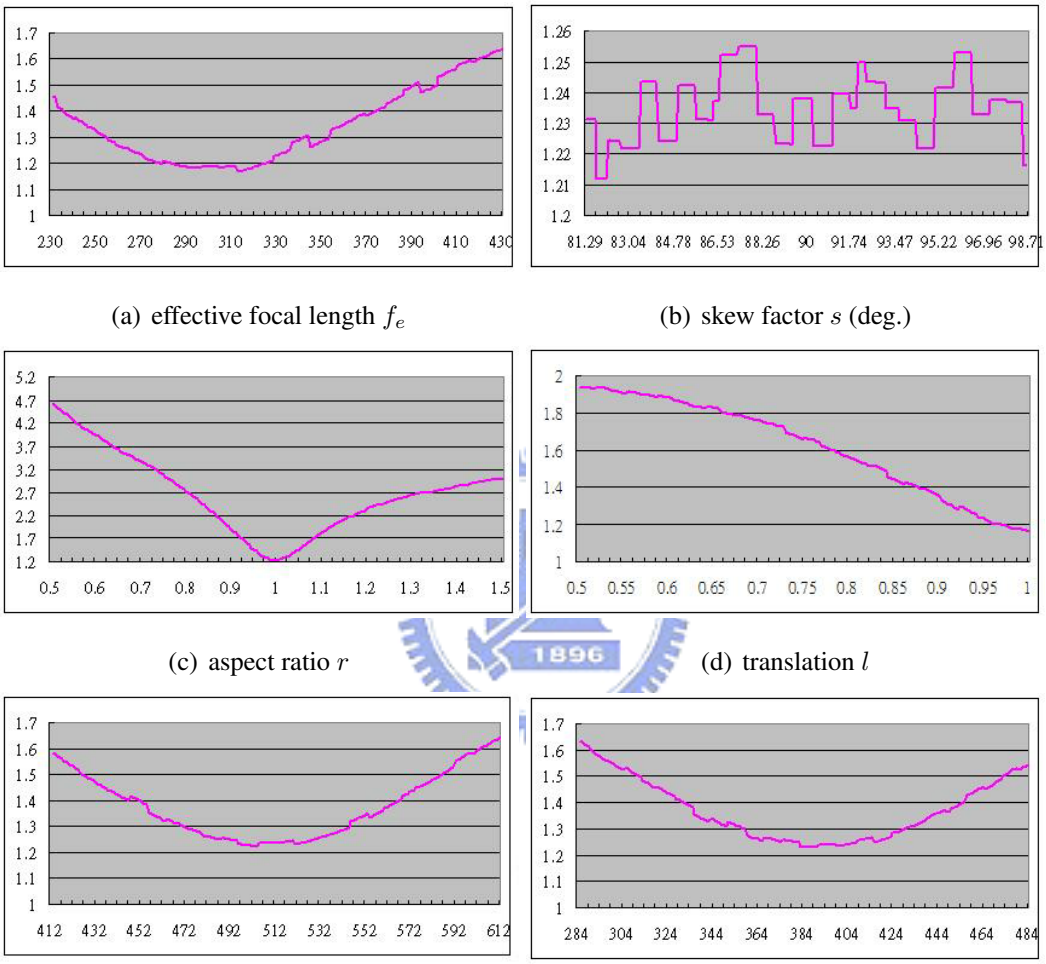

(a) effective focal length f_e

(b) skew factor s (deg.)

(c) aspect ratio r

(d) translation l

(e) principal point u_0 (pixel)

(f) principal point v_0 (pixel)

Figure 5.4: **The influence of parameters in VSM to the objective function** ($\sigma = 1$)**.**

	(u_0, v_0)	r	s	f_e	l	Error(pixel)
Ground truth	(512,384)	1.000	0.000	330.000	0.950	0.161 *
Initial guess(1)	(512,384)	1.000	0.000	330.000	0.950	0.161
Ours	(512,383)	1.000	0.002	330.851	0.950	0.099
Ying's	(525,380)	1.000	0.001	344.195	0.950	0.391
Initial guess(2)	(532,364)	1.000	0.000	330.000	0.950	0.592
Ours	(513,383)	1.000	0.007	332.758	0.949	0.113
Ying's	(523,370)	1.001	0.000	360.851	0.950	0.734
Initial guess(3)	(532,364)	1.000	0.000	350.000	0.950	0.678
Ours	(512,384)	0.999	0.000	328.843	0.953	0.116
Ying's	(523,370)	1.001	0.000	360.851	0.950	0.734
Initial guess(4)	(600,300)	1.000	0.000	430.000	0.850	13.379
Ours	(512,382)	0.999	-0.093	328.477	0.950	0.119
Ying's	(526,380)	1.000	0.000	583.851	0.849	6.247

Table 5.3: **Simulation result of central catadioptric camera calibration with different initial guess.**

cedure. Conclusively, the proposed optimization procedure is robust than the one proposed by Ying.

Notice that the calibration error of the ground truth is $0.161234(pixel)$ rather than $0(pixel)$. This error is generated during the process of feature extraction. We estimate the coordinate of feature points by calculating the mass center of the circle. However, the feature points in the virtual perspective image are elliptic rather than circular. Therefore, the coordinate of the feature points will be shifted.

5.1.2 Real Experiment

It is necessary to apply the proposed method in real experiment, then the calibrated camera can be used in many vision applications. However, we never have the ground truth for the catadioptric camera. Therefore, we only evaluate the performance by calculating

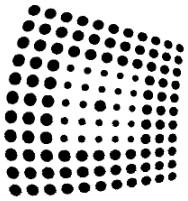

(a) Simulation data

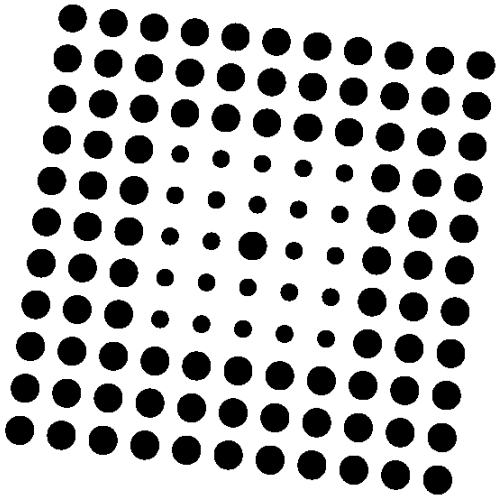

(b) Its virtual perspective image

Figure 5.5: **Simulation image contains one calibration pattern and the virtual perspective image constructed using the ground truth.**

the calibration error in this section.

Before the experiment, it is important to verify whether the perspective camera and the mirror of the catadioptric camera we used are perfectly aligned. Therefore, we introduce a method based on pose estimation to align the camera and the mirror of catadioptric camera in appendix B. After the verification, we start to calibrate the central catadioptric camera in the following. First, we estimate a set of initial parameters in VSM for the central catadioptric camera by combining the parameters of the perspective camera and the mirror. Afterwards, we optimize the parameters in viewing sphere model using the proposed optimization procedure.

Initial Camera Parameters Estimation

In the following, we estimate the initial parameters in viewing sphere model by combining the parameters of hyperboloidal mirror and perspective camera. The surface of hyperboloidal mirror we used can be described as following equation, $\frac{x^2+y^2}{a^2}+\frac{z^2}{b^2}=-1$ where $a=67.08, b=150.00$, and the eccentricity of the hyperboloid is $\sqrt{1+\frac{b^2}{a^2}}=1.095439$. The intrinsic parameters of perspective camera are estimated using Zhang's calibration method for perspective camera [50]. According to these parameters, the initial parameters of viewing sphere model can be estimated and the result is shown in the following.

Principal point (u_0, v_0) The principal point of central catadioptric camera is the same as the principal point of the perspective camera. Hence, the initial value of the principal point (u_0, v_0) is $(547.748672, 393.819871)$.

Skew factor s The skew factor of central catadioptric camera is the same as the skew factor of the perspective camera. Hence, the initial value of the skew factor s is 0.

Aspect ratio r The aspect ratio of central catadioptric camera is the same as the aspect ratio of the perspective camera. Hence, the initial value of the aspect ratio r is 0.997324.

Translation l The translation of central catadioptric camera can be obtained from the eccentricity of the hyperboloid. Hence, the translation is $l=\frac{2\varepsilon}{1+\varepsilon^2}=0.995859$.

	(u_0, v_0)	r	s	f_e	l	Error(pixel)
Initial	(547,393)	0.997	0.000	330.834	0.995	1.277
Optimized	(530,393)	1.008	-0.003	328.041	0.999	0.887

Table 5.4: **Result of proposed calibration method for central catadioptric camera.**

Effective focal length f_e The effective focal length of central catadioptric camera can be obtained from the focal length of the perspective camera and the eccentricity of the hyperboloid. Hence, the effective focal length is $f_e = -\frac{1-\varepsilon^2}{1+\varepsilon^2} f = 330.834591$.

Camera Parameters Optimization

After estimating the initial parameters of viewing sphere model, we refine the parameters using our optimization procedure. In real experiment, we take images of calibration pattern we designed for 7 times and calculate virtual perspective image of each calibration pattern by the initial parameters of viewing sphere model (figure 5.6). The resolution of virtual perspective image is 1024×768 and the parameters of the virtual perspective camera are shown below, image coordinate of principal point is $(512, 386)$; aspect ratio is 1; skew factor is 0; and focal length is 500. After the construction of virtual perspective image, we can optimize the parameters of viewing sphere model by minimizing the calibration error of feature points extracted from the planar pattern. The optimization procedure is implemented by Powell's method [18]. The results are shown in table 5.5. To demonstrate the performance of proposed method, we also give a bad initial parameters, and the result also converge to the same parameters. The perspective image of the initial and optimized parameter are shown in figure 5.7. The virtual perspective image constructed by initial parameters is distorted. After the optimization process, the virtual perspective image constructed by the optimized parameters is more like perspective image.

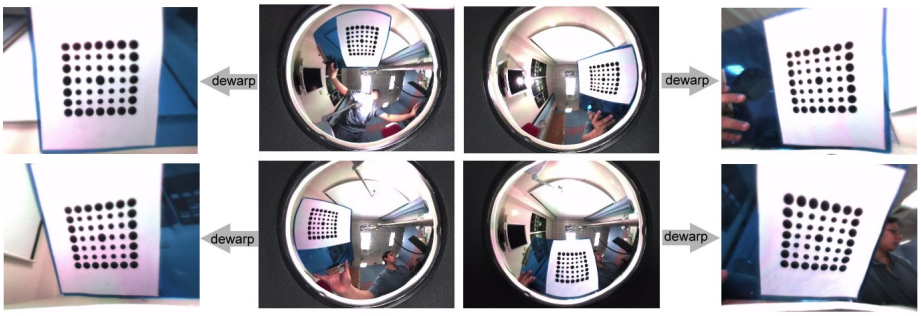

Figure 5.6: **Real images in our experiment for central catadioptric camera calibration.** For better accuracy of camera calibration, the calibration patterns had better be distributed all over the image and the number of the calibration patterns appearing in the image should be as many as possible. Hence, we take images of planar pattern for seven times in different directions in real experiment.

	(u_0, v_0)	r	s	f_e	l	Error(pixel)
Initial	(547,393)	1.000	0.000	530.000	0.800	4.729
Optimized	(547,393)	1.006	-0.005	368.196	0.994	1.197

Table 5.5: **Result of proposed calibration method for central catadioptric camera.**

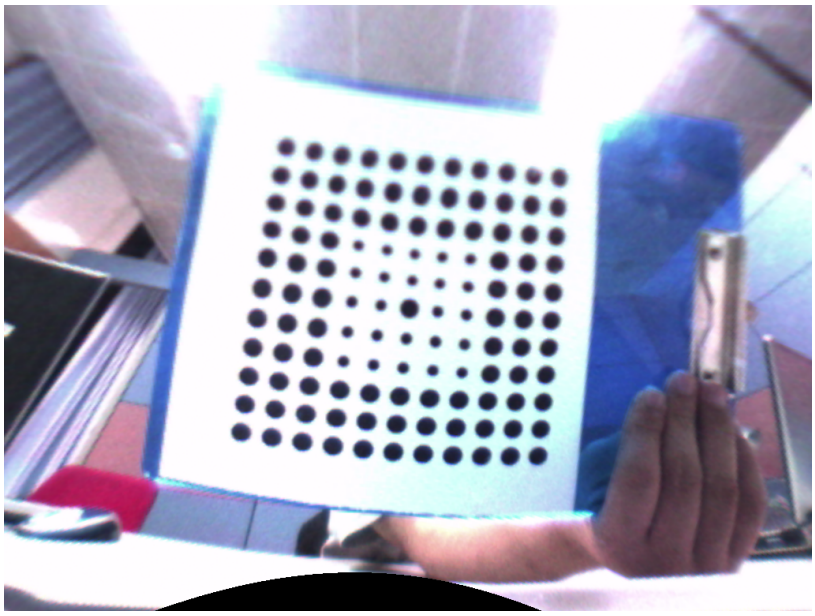

(a) Virtual perspective image of initial parameters

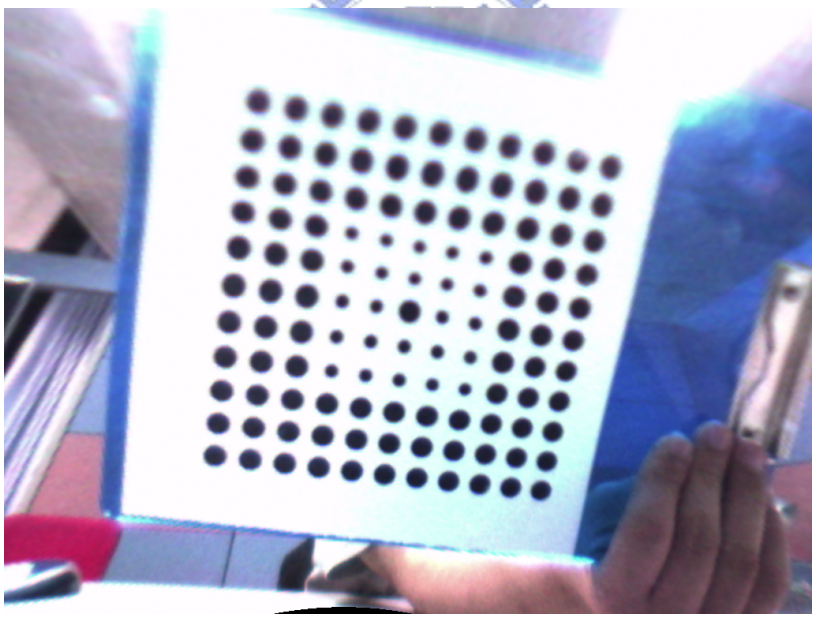

(b) Virtual perspective image of optimized parameters

Figure 5.7: **Virtual perspective images constructed by the initial guess and the optimized parameters.**

	(u_0, v_0)	r	s	f_e	l	Error(pixel)
GT	(512,384)	1.000	0.000	300.000	0.995	none
1	(512,384)	1.000	0.000	299.983	0.995	0.001
3	(512,384)	1.000	0.000	299.983	0.995	0.004
5	(512,384)	1.000	0.000	299.987	0.995	0.003
6	(512,384)	1.000	0.000	299.983	0.995	0.003

Table 5.6: **Calibration Results with diffident numbers of calibration pattern ($\sigma = 0$).**

5.1.3 Discussions

Number of calibration patterns

To obtain precise calibration result, the calibration patterns had better be distributed all over the image and the number of the calibration patterns appearing in the image should be as many as possible. If the calibration patterns are appeared in partial image rather than distributed all over the image, can we still obtain correct calibration result? We perform the simulation result with $1, 3, 5, 7$ planar patterns and the results are shown in the following tables (table 5.6 and table 5.7). When there is no noise, we can still estimate precise camera parameters with a few number of calibration patterns. But, when we add gaussian noise ($\sigma = 1$) to the simulation data, the calibration result with more calibration patterns is better than one with less calibration patterns. To obtain more precise calibration result, we recommend capture more images of the calibration pattern during the calibration experiment.

Performance comparison with Ying's method

In the results of simulation experiment, we compare the performance of our calibration method with Ying's calibration method. The results show that our calibration result is worse than Ying's when the noise level is higher than $\sigma = 0.4$. However, the comparison is unfair. In the case of Ying's simulation data, the noise is added to each point on the edge of the conic. When we add high level noise to these points, the fitted conic is almost the

	(u_0, v_0)	r	s	f_e	l	Error(pixel)
GT	(512,384)	1.000	0.000	300.000	0.995	none
1	(534,413)	1.001	-2.551	319.053	1.000	1.112
3	(518,390)	0.996	1.315	310.545	1.000	0.378
5	(517,394)	0.992	-1.426	314.539	1.000	0.229
6	(517,400)	0.997	0.941	311.490	1.000	0.166

Table 5.7: **Calibration Results with diffident numbers of calibration pattern ($\sigma = 1$).**

same with the original conic (the ground truth). But in the case of our simulation data, we add the noise directly to each feature point on the image. When we add high level noise to these points, the shape of the grid will be distorted seriously. Therefore, the comparison is unfair and we cannot add the noise to each point directly.

Our solution is adding the noise proportionably to the circle boundary of each feature point, and the coordinate of feature point can be calculated by the mass center of the all points on the circle boundary. Because the noise which we add is zero mean, the calculated coordinate of the feature point should be the same with the original one (the ground truth).

5.2 Results of Non-central Catadioptric Camera Calibration

In this section, we evaluate the performance of our calibration method for non-central catadioptric camera by simulation and real experiment.

5.2.1 Simulation Experiment

In our calibration method for non-central catadioptric camera, we need a calibrated central catadioptric camera to estimate the 3D point coordinate. Therefore, we generate simulation data for both central and non-central catadioptric camera. Both simulation data are both generated using the reflected ray model. We generate three sets of simulation

	(u_0, v_0)	r	s	f	(a, b)	$mirrorpose$
central.	(512,384)	1	0	3300	(67.08,150)	$\begin{bmatrix} 1 & 0 & 0 & 0 \\ 0 & 1 & 0 & 0 \\ 0 & 0 & 1 & c \end{bmatrix}$
Noncentral.	(512,384)	1	0	1500	(67.08,150)	$\begin{bmatrix} 1 & 0 & 0 & 0 \\ 0 & 1 & 0 & 0 \\ 0 & 0 & 1 & 0 \end{bmatrix}$

Table 5.8: **Ground truth of simulation data for non-central catadioptric camera calibration.**

images shown on LCD, and the distance between the image plane of simulation data and the origin of the mirror is about $640mm$. The ground truth of the parameters for the central and non-central catadioptric camera is shown in table 5.8. The procedure of simulation data generation are also described in appendix A.

In the simulation data, gaussian noise with zero-mean and σ standard deviation is added to the image points of both central and non-central catadioptric camera. We vary the noise level σ from 0.0 to 2.0 pixels. Then, we evaluate the performance of our calibration method for non-central catadioptric camera using the simulation data. In this simulation, we discuss two cases of conditions in the calibration procedure, the first condition is that **the perspective camera is calibrated and the parameters of the mirror is known**, and the second condition is that **the perspective camera is not calibrated and the parameters of the mirror is known**.

For the case of both the parameters of the perspective camera and the mirror are known, the results of simulation experiment are shown in table 5.9. We estimate the initial mirror posture by Mashita's method which using the mirror boundary. The results show that the calibration error is large when the noise level is high. But, the estimated relative pose between perspective camera and mirror is still close to the ground truth. According to the result, it shows that the proposed method is accurate and robust in the case of the perspective camera is calibrated and the parameters of the mirror is known.

For the case of that the perspective camera is uncalibrated, the results are shown in

Noise level	R_x (deg.)	R_y (deg.)	R_z (deg.)	Translation (mm)	Error(mm)
GT	0.000	0.000	0.000	(0.000, 0.000, 0.000)	
0	0.878	0.319	-0.140	(-0.930, 2.571,-0.305)	2.021
0.4	0.868	0.320	-0.145	(-0.931, 2.538,-0.483)	3.408
0.8	0.893	0.321	-0.132	(-0.932, 2.607,-0.396)	5.550
1.2	0.857	0.322	-0.145	(-0.931, 2.507,-0.578)	8.022
1.6	0.902	0.323	-0.567	(-0.932, 2.581,-0.679)	10.864
2.0	0.925	0.327	-0.501	(-0.913, 2.574,-0.905)	13.647

Table 5.9: **Simulation result of non-central catadioptric camera calibration (case 1).**

Noise level	f	s	r	(u_0, v_0)	R_x (deg.)	R_y (deg.)	R_z (deg.)	Translation (mm)	Error(mm)
0	1437.737	-16.270	1.006	(524,381)	1.028	0.865	-0.612	(-0.950, 2.553,-7.174)	0.928
0.4	1439.579	-12.387	1.007	(525,381)	1.025	0.873	-0.465	(-0.948, 2.574,-6.914)	2.963
0.8	1438.578	-13.224	1.005	(524,381)	1.037	0.862	-0.409	(-0.953, 2.586,-7.153)	5.481
1.2	1428.968	-8.869	1.007	(524,381)	1.024	0.863	-0.331	(-0.960, 2.575,-8.591)	8.426
1.6	1434.107	-8.090	1.002	(524,381)	1.026	0.860	-0.220	(-0.943, 2.623,-8.410)	10.832
2.0	1439.398	1.483	0.997	(525,381)	1.041	0.880	-0.144	(-0.933, 2.657,-8.646)	12.340

Table 5.10: **Simulation result of non-central catadioptric camera calibration (case 2).**

table 5.11. We also estimate the initial mirror posture by Mashita's method which using the mirror boundary. The estimated calibration error of this case is almost the same with the calibration error of above case. But, the estimate parameters are not accurate because there are too many unknown parameters in this case. In a conclusion, we can obtain better camera parameters if the perspective camera is calibrated in advance. In the case of that camera parameters of the perspective camera is unknown, the initial estimation of perspective camera is very important. Using good initial camera parameters, there is more chance to estimate correct camera parameters. Otherwise, it will be trap in a local minimum.

The same with simulation experiment of central catadioptric camera calibration, we

	R_x (deg.)	R_y (deg.)	R_z (deg.)	Translation (mm)	Error(mm)
Ground truth	0.000	0.000	0.000	(0.000, 0.000, 0.000)	5.692
Initial guess(1)	0.000	0.000	0.000	(0.000, 0.000, 0.000)	5.692
Relative pose	-0.030	0.028	-0.010	(-0.000,-0.003, 0.078)	1.087
Initial guess(2)	0.000	0.000	0.000	(0.000, 0.000, 10.000)	31.055
Relative pose	-0.037	0.018	-0.029	(0.021,-0.023, 0.152)	1.075
Initial guess(3)	0.000	0.000	0.000	(0.000, 0.000,100.000)	292.227
Relative pose	-0.043	-0.101	-0.005	(0.371,-0.038, 0.238)	1.119
Initial guess(4)	5.732	5.732	5.732	(0.000, 0.000, 0.000)	738.396
Relative pose	-0.411	0.064	0.047	(-0.105,-1.121, 0.048)	1.402

Table 5.11: **Simulation result of non-central catadioptric camera calibration with different initial guess.**

also generate simulation data by the projection of a virtual calibration pattern in space to evaluate the performance of the feature extraction in our method. By comparing the results of two sets of simulation data, we can estimate the error generated during the process of feature extraction in image based simulation data. In image based simulation data, we generate a set of central and non-central catadioptric images. The simulated images are shown in figure 5.8.

For the verification of the performance of the calibration method, we set several different initial parameters in the simulation experiment. The results are shown in table 5.11. The simulation results show that the mirror posture estimated by our method converge to the ground truth. The calibration error is also minimized. The same condition as the simulation result for central catadioptric camera, the calibration error of the ground truth is $5.692mm$. The error is also generated during the process of feature extraction.

5.2.2 Real Experiment

In this section, we calibrate a non-central catadioptric camera (MAPCAM made by company EERISE) by our calibration method for non-central catadioptric camera. At first,

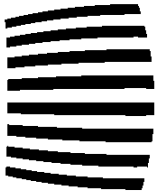

(a)

(b)

Figure 5.8: **Simulated image contains special pattern shown on LCD (one kind of eight).**

	f	s	r	(u_0, v_0)	R_x (deg.)	R_y (deg.)	R_z (deg.)	Translation (mm)	Error(mm)
initial parameter	517.857	0.000	1.000	(320,240)	0.000	0.000	0.000	(-6.938, 1.295, -97.784)	163.189
optimized result	518.101	-4.248	0.964	(317,243)	0.006	0.050	0.036	(-1.955, 1.842, -107.640)	7.314

Table 5.12: **Result of proposed calibration method for non-central catadioptric camera.**

we estimate the 3D coordinate of the feature points on LCD by a calibrated central catadioptric camera, and the correspondence between central and non-central catadioptric images. In the real experiment, we use 3 LCDs in different orientations. The result is shown in figure 5.9. There are 576 feature points generated both in central and non-central catadioptric images. After estimating the feature points, we have to find the correspondence of the feature points. As aforementioned, we find the corresponding points by matching the bitcode of each feature point. Feature points which have the same bitcode are the corresponding points between non-central and central catadioptric images.

Next, we calibrate the non-central catadioptric camera using the estimated corresponding points. Because the perspective camera is sealed inside the non-central catadioptric camera, we cannot estimate the intrinsic parameters of the perspective camera. Therefore, we estimate the initial parameters for the perspective camera by the specification of the camera. The initial relative pose between the camera and the mirror is estimated by Mashita's method [48] which using the mirror boundary. The initial parameters and the optimized results are in the table 5.12. The calibration error of initial parameters estimated by Mashita's method is large. Using our optimization procedure, the calibration error is reduced significantly.

5.2.3 Discussions

The influence of number of unknown parameters for reflected ray model

There are totally 13 unknown variables in the reflected ray model, including 5 unknown variables for the perspective camera, 6 unknown variables for the transformation matrix and 2 unknown variables for the reflective mirror. If above variables are all unknown, it

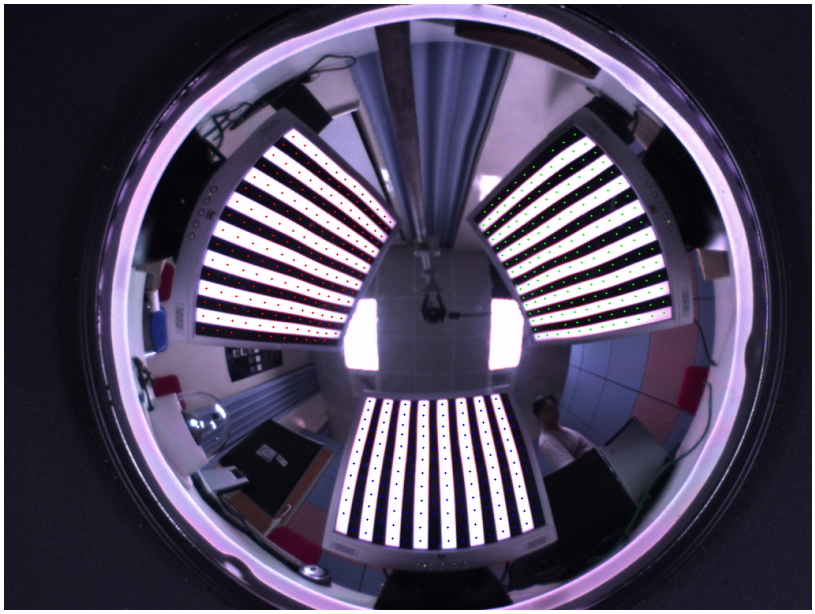

(a) Central catadioptric image

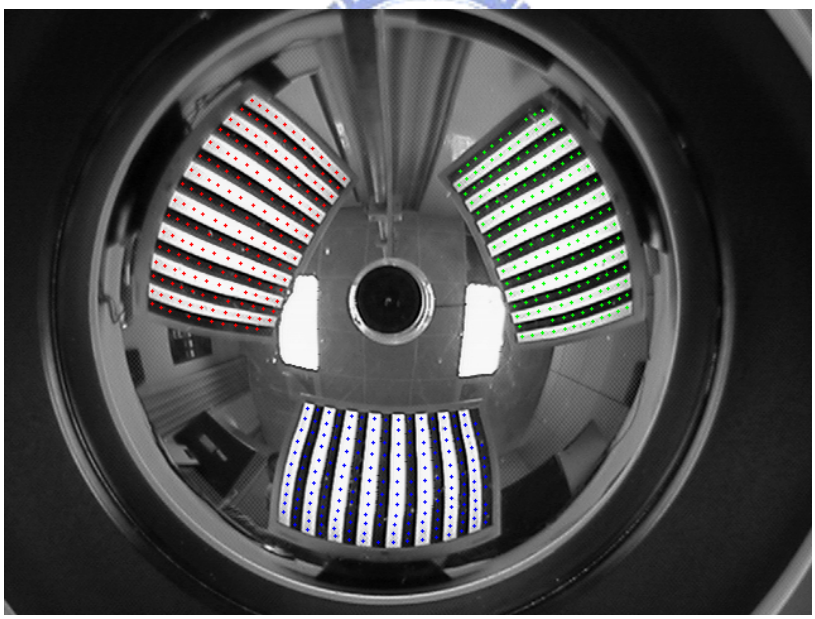

(b) Non-central catadioptric image

Figure 5.9: **Feature points generated by image patterns shown on LCDs.** In the real experiment, we will use 3 LCDs. And there are 576 feature points generated both in non-central and central catadioptric images.

is very difficult to estimate precise camera parameters. If we can calibrate the perspective camera and examine the parameters of the mirror in advance, we only have to estimate the transformation matrix between the perspective camera and the reflective mirror. The transformation matrix only have 6 variables needed to be solved, and we can estimate the initial parameters by Mashita's method and refine the parameters by proposed optimization procedure. Then, we can estimate precise parameters of each component.

The influence of incorrect camera parameters of central catadioptric camera

In our calibration method for non-central catadioptric camera, we estimate the 3-D coordinate of feature points on LCD by a calibrated central catadioptric camera. In the real experiment, we can never find a central catadioptric camera because it is impossible to align the perspective camera and the reflective mirror perfectly. We only can align the perspective camera and the reflective mirror as precise as possible. Hence, there must be errors for the parameters of central catadioptric camera and the 3-D coordinate of the feature points on LCD. This will influence the calibration result of non-central catadioptric camera. However, the error is inevitable. All we can do is to align the perspective camera and the reflective mirror as precise as possible and perform the experiment as careful as possible.

5.3 An Application of Catadioptric Camera Calibration : Robot Navigation

In this section, we use the non-central catadioptric camera which is calibrated by proposed calibration method in the application of robot navigation to demonstrate the performance of proposed calibration method.

As aforementioned, there must be blind spots for the camera which is located at a fixed location because of the problem of occlusion. One solution to the problem is to setup the camera on a mobile robot. In this way, we can change the viewpoint of the camera by controlling the mobile robot. The problem of the robot navigation is to guide the mobile robot to the place we desired. Then, we can control the robot to execute the mission we

Navigation method	error (%)	Error accumulation
No calibration	$8\% \sim 10\%$	yes
mechanic based method	$1\% \sim 3\%$	yes
Vision based method	$1\% \sim 3\%$	no

Table 5.13: **Comparison of methods for navigation.**

instructed.

In conventional mobile robot, there is an odometer on the robot to maintain its current position. But, the position maintained by the odometer is not always the same with real position of the mobile robot due to the mechanic error of the mobile robot, and the error accumulates while the robot moves. Classical mechanic based methods compensate the error by measuring the error generated when the robot moves in advance. In this way, the mechanic error can be reduced. However, there are still errors in this method, and the error will accumulates while the mobile robot keep moving. There is an old saying "Outsiders see more than insiders". In vision based method, there is a camera which can see the patrolling environment to navigate the mobile robot. The vision based methods for robot navigation are efficient because the error does not accumulate (table 5.13). Due to large field of view for catadioptric camera, it is suitable in this application.

The mobile robot used in this application is the **Amigo Robot** made by ActivMedia Robotics Technologies, Inc (figure 5.10). The size of the robot is $33cm \times 28cm \times 21cm$. There is a network camera, (AXIS 213 PTZ) carried on the robot, and images captured by the camera can be transferred to a server through wireless network. The environment where the mobile robot patrols is shown in Figure 5.11, and the calibrated non-central catadioptric camera is set on the ceiling of the environment. The scenario of this application is as following. First, we click one point in the catadioptric image, then the robot will go to the corresponding position of the clicked point on the floor. To actualize the scenario, we propose a method to navigate the mobile robot, and the navigation procedure has two steps as following.

Relative pose between image coordinate and robot coordinate At first, we need to esti-

Figure 5.10: **The mobile robot in the application of robot navigation.**

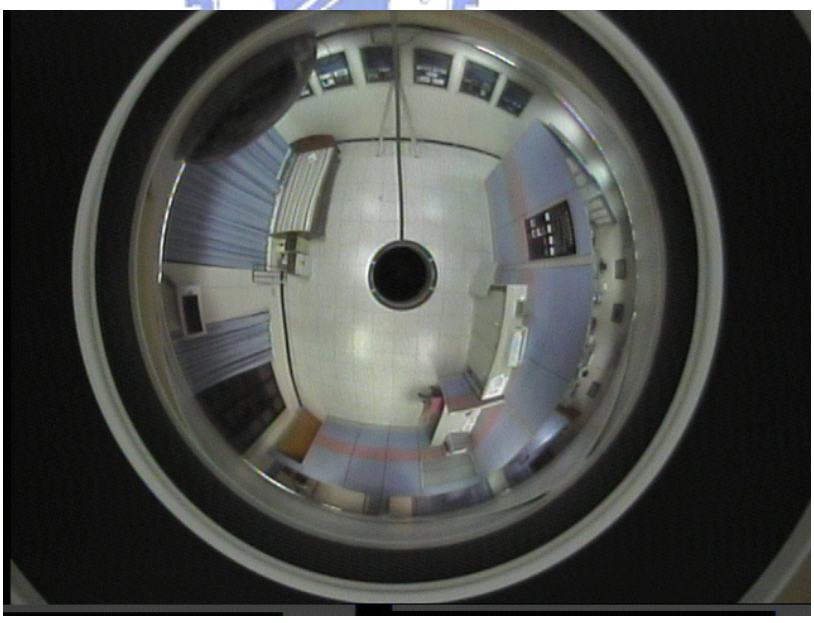

Figure 5.11: **Demo site for robot navigation.**

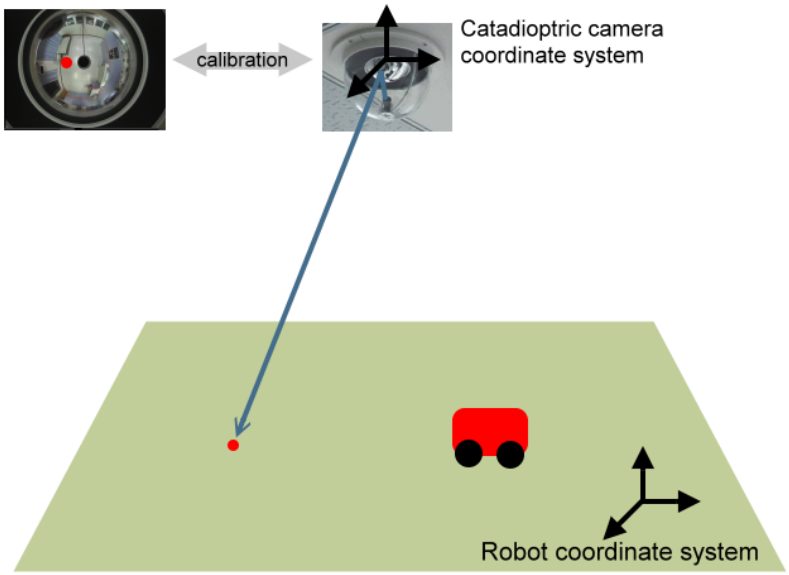

Figure 5.12: **Vision based method for robot navigation.** We use a calibrated catadioptric camera to navigate the mobile robot. First, we estimate the relative pose between the camera and the floor (the robot). Next, we can calculate the corresponding point on the floor for each image point using the camera parameters and estimated relative pose. Then, we can navigate the mobile robot by the catadioptric camera.

mate the relative pose between the coordinate system of catadioptric camera and the one of the robot (or the floor coordinate system). Because the catadioptric camera is calibrated, we can estimate the relative pose by clicking a sets of corresponding points between image and floor.

The mapping between image coordinate and robot coordinate After the estimation of the relative pose, we can calculate the corresponding floor point of each pixel in catadioptric image by two steps. In the first step, we calculate the corresponding light ray of the clicked pixel by the camera parameters of the catadioptric camera. In the second step, we change the coordinate system of the light ray from the catadioptric camera to the robot. Then, we can calculate the intersection of the light ray and the plane of the floor, and the intersection is the corresponding point of the clicked point in catadioptric image (figure 5.12).

We apply the proposed method for robot navigation in an application of surveillance. In this demonstration, there is an intruder walking into the demo site and try to steal something on the bed. The surveillance system will detect the intruder and control the PTZ camera to capture high solution images of the intruder. When the intruder is stealing some valuable object on the bed, the system alarms and we navigate the robot to approach the intruder (figure 5.13). Then, the intruder aware he has been detected and run away. There are many technologies in this demonstration, including background modeling, camera calibration and interfaces of the mobile robot. In this application, we apply proposed calibration method to navigate the mobile robot, and demonstrate the performance of proposed calibration method.

(a) (b)

(c) (d)

(e) (f)

Chapter 6

Conclusion

In this thesis, we propose two novel calibration methods to estimate the intrinsic parameters of central and non-central catadioptric camera systems using planar calibration objects.

For central catadioptric camera, we propose a novel calibration method using a planar calibration pattern in chapter 3. It only requires the catadioptric camera to observe the planar pattern shown at a few different orientations. Compared with conventional photogrammetric calibration methods, our method is more **flexible** and easy to use.

For non-central catadioptric camera, we propose a novel calibration method using a calibrated central catadioptric camera and LCD in chapter 4. In the calibration procedure, we use the calibrated central catadioptric camera to estimate the relative pose between mirror of central catadioptric camera and LCD. Then, we replace the central catadioptric with the non-central catadioptric camera to obtain the coordinate of 3D world points. The correspondence of 2D image points and 3D world points is estimated automatically by 20 different patterns shown on LCD. Compared with conventional calibration methods, our method is more **efficient**.

In chapter 5, the simulation is conducted to generate data with the ground truth for verification and demonstration of the proposed methods. For central catadioptric camera, the results show that our method is **robust** and **accurate**, and the performance of our method is better than calibration method using geometric invariants. For non-central catadioptric camera, the results show that our method is **robust** and **accurate**, and the performance of our method is better than calibration method proposed by Mashita using the mirror boundary. Besides, we also calibrate a central catadioptric camera (combined by Marlin F-080C and a hyperbolic mirror) and a non-central catadioptric camera (MAPCAM) by using our calibration method. Finally, we navigate a mobile robot (Amigo Robot) using the calibrated non-central catadioptric camera to demonstrate the performance of proposed calibration method.

Bibliography

[1] A. Krishnan Ahuja and N. Panoramic image acquisition. *Proc. of IEEE Conf. on Computer Vision and Pattern Recognition*, 1996.

[2] D. Aliaga. Accurate catadioptric calibration for real-time pose estimation in room-size environments. *Proceedings of the International Conference on Computer Vision*, pages 127–134, 2001.

[3] J. Barreto Araujo and H. Issues on the geometry of central catadioptric image formation. *Proceedings of the IEEE Conference on Computer Vision and Pattern Recognition*, 2001.

[4] J. P. Barreto Araujo and H. Geometric properties of central catadioptric images. *Proceedings of European Conference on Computer Vision*, 2002.

[5] J. P. Barreto Araujo and H. Paracatadioptric camera calibration using lines. *Proceedings of the International Conference on Computer Vision*, 2003.

[6] J. P. Barreto Araujo and H. Geometric properties of central catadioptric line images and their application in calibration. *IEEE Transactions on Pattern Analysis and Machine Intelligence*, 27:1327–1333, 2005.

[7] S. K. Nayar Baker and S. Catadioptric image formation. *Proc. of DARPA Image Understanding Workshop*, 1997.

[8] L. McMillan Bishop and G. Plenoptic modeling: An image-based rendering system. *Computer Graphics: Proc. of SIGGRAPH 95*, pages 39–46, 1995.

[9] C. K. Yu C. S. Chen and Y. P. Hung. New calibration-free approach for augmented reality based on parameterized cuboid structure. *Proceedings of the IEEE International Conference on Computer Vision*, pages 30–37, 1999.

[10] S. E. Chen. Quicktime vr - an image based approach to virtual environment navigation. *Computer Graphics: Proc. of SIGGRAPH 95*, pages 29–38, 1995.

[11] Microsoft Corp. Msdn library.

[12] S. D. Zimmermann D. P. Kuban, H. L. Martin and N. Busico. Omniview motionless camera surveillance system. *United States Patent No. 5,359,363*, 1994.

[13] C. Geyer Daniilidis and K. Catadioptric camera calibration. *Proceedings International Conference on Computer Vision*, pages 398–404, 1999.

[14] C. Geyer Daniilidis and K. A unifying theory for central panoramic systems. *Proceedings of European Conference on Computer Vision*, pages 445–462, 2000.

[15] C. Geyer Daniilidis and K. Catadioptric projective geometry. *International Journal of Computer Vision*, 45(3):223–243, 2001.

[16] C. Geyer Daniilidis and K. Paracatadioptric camera calibration. *IEEE Transactions on Pattern Analysis and Machine Intelligence*, 4:1–10, 2002.

[17] S. J. Maybank Faugeras and O. D. A theory of selfcalibration of a moving camera. *The International Journal of Computer Vision*, 8:123–152, 1992.

[18] W. H. Press Flannery, S. A. Teukolsky, W. T. Vetterling, and B. P. Numerical recipes in c. *Cambridge University Press*, 1989.

[19] A. Goshtasby Gruver and W. A. Design of a single-lens stereo camera system. *Pattern Recognition*, 26(6):923–937, 1993.

[20] S. J. Oh Hall and E. L. Guidance of a mobile robot using an omnidirectional vision navigation system. *Proc. of the Society of Photo-Optical Instrumentation Engineers*, 1987.

[21] J. Hong. Image based homing. *Proc. of IEEE International Conference on Robotics and Automation*, 1991.

[22] X. Ying Hu and Z. Catadioptric camera calibration using geometric invariants. *Proc. International Conference on Pattern Recognition*, 2, 2003.

[23] X. Ying Hu and Z. Can we consider central catadioptric cameras and fisheye cameras within a unified imaging model. *Proc. European Conference on Computer Vision*, 2004.

[24] X. Ying Hu and Z. Catadioptric camera calibration using geometric invariants. *IEEE Transactions on Pattern Analysis and Machine Intelligence*, 26:1260–1271, 2004.

[25] Y. S. Chen K. W. Chen, Y. P. Hung. On calibrating a camera network using parabolic trajectories of a bouncing ball. *Proceedings of the Second Joint IEEE International Workshop on Visual Surveillance and Performance Evaluation of Tracking and Surveillance*, 2005.

[26] Y. Yagi K. Yamazawa and M. Yachida. Obstacle avoidance with omnidirectional image sensor hyperomni vision. *Proc. of IEEE International Conference on Robotics and Automation*, pages 1062–1067, 1995.

[27] S. B. Kang. Catadioptric self-calibration. *Proceedings of the IEEE Conference on Computer Vision and Pattern Recognition*, 1, 2002.

[28] Y. Yagi Kawato and S. Panoramic scene analysis with conic projection. *Proc. of International Conference on Robots and Systems*, 1990.

[29] D. C. Lay. *Linear Algebra and its applications*. Addison Wesley, 1998.

[30] Open Source Computer Vision Library. http://www.intel.com/technology/computing/opencv/.

[31] Q. T. Luong. *atrice Fondamentale et Calibration Visuelle surl' Environment-Vers une plus grande autonomie des system robotiques*. PhD thesis, 1992.

[32] P. Sturm Maybank and S. On plane-based camera calibration: A general algorithm, singularities, applications. *Proceedings of the IEEE Conference on Computer Vision and Pattern Recognitions*, pages 432–437, 1999.

[33] V. Nalwa. A true omnidirectional viewer. *Technical report, Bell Laboratories, Holmdel, NJ 07733, U.S.A.*, 1996.

[34] M. D. Grossberg Nayar and S. K. A general imaging model and a method for finding its parameters. *Proceedings of the International Conference on Computer Vision*, pages 108–115, 2001.

[35] S. Baker Nayar and S. K. A theory of catadioptric image formation. *Proceedings of the International Conference on Computer Vision*, pages 35–42, 1998.

[36] S. K. Nayar. Sphereo: Recovering depth using a single camera and two specular spheres. *Proc. of SPIE: Optics, Illmumination, and Image Sensing for Machine Vision*, 1988.

[37] Shree K. Nayar. Catadioptric omnidirectional camera. *Proceedings of the IEEE Conference on Computer Vision and Pattern Recognition*, 1997.

[38] B. Micusik Pajdla and T. Autocalibration and 3d reconstruction with non-central catadioptric cameras. *Proceedings of the IEEE Conference on Computer Vision and Pattern Recognition*, 1:58–65, 2004.

[39] B. Mucusik Pajdla and T. Para-catadioptric camera autocalibration from epipolar geometry. *Proceedings of Asian Conference on Computer Vision*, 2:748–753, 2004.

[40] M. D. Grossberg R. Swaminathan and S. K. Nayar. Caustics of catadioptric cameras. *Proceedings of the International Conference on Computer Vision*, 2001.

[41] D. Strelow Singh, J. Mishler, D. Koes, and S. Precise omni-directional camera calibration. *Proceedings of the IEEE Conference on Computer Vision and Pattern Recognition*, pages 689–694, 2000.

[42] H. L. Chou Tsai and W. H. A new approach to robot location by house corners. *Pattern Recognition*, 19:439–451, 1986.

[43] R. Y. Tsai. A versatile camera calibration technique for high-accuracy 3d machine vision metrology using off-the-shelf tv camera and lenses. *IEEE Journal of Robotics and Automation*, 3:323–344, 1987.

[44] S. W. Jeng Tsai and W. S. Precise image unwarping of omnidirectional cameras with hyperbolic-shaped mirrors. *CVGIP*, pages 414–422, 2003.

[45] S. W. Jeng Tsai and W. S. Construction of perspective and panoramic images from omni-images taken from hypercatadioptric cameras for visual surveillance. *Proceedings of the 2004 IEEE Internatmat Conference an Networking, Sensmg and Control*, pages 204–209, 2004.

[46] J. Y. Zheng Tsuji and S. Panoramic representation of scenes for route understanding. *Proc. of the Tenth International Conference on Pattern Recognition*, 1:161–167, 1990.

[47] R. C. Gonzalez Woods and R. E. *Digital Image Processing*. Prentice Hall, 2002.

[48] T. Mashita Yachida, Y. Iwai, and M. Calibration method for misaligned catadioptric camera. *The 6th Workshop on Omnidirectional Vision, Camera Networks and Non-classical cameras*, 2005.

[49] K. Yamazawa Yachita, Y. Yagi, and M. Omnidirectional imaging with hyperboloidal projection. *Pro. of IEEE/RSJ International Conference on Intelligent Robots and Systems*, 2(1029-1034), 1993.

[50] Z. Zhang. A flexible new technique for camera calibration. *IEEE Transactions on Pattern Analysis and Machine Intelligence*, 22:1330–1334, 2000.

[51] Z. Y. Zhang. Camera calibration with one-dimensional objects. *IEEE Transactions on Pattern Analysis and Machine Intelligence*, 26:892–899, 2004.

Appendix A

Simulation Data Generation

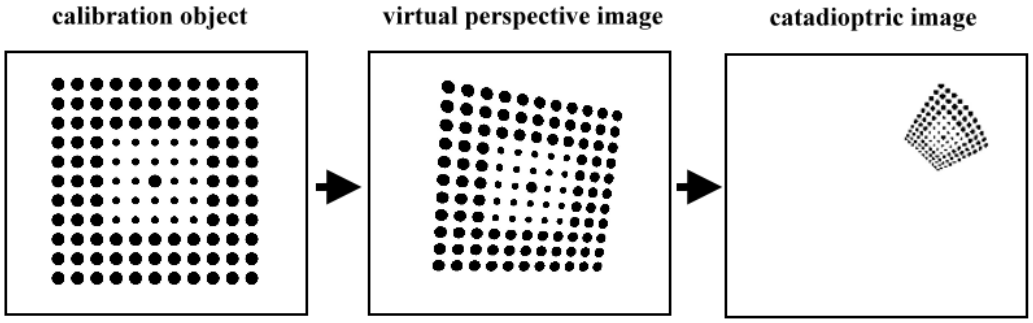

Figure A.1: **Simulation data generation for central catadioptric camera calibration.**

A.1 Simulation Data for Central Catadioptric Camera

We generate simulation data for central catadioptric camera calibration by three steps (figure A.1). In the first step, we generate a set of feature points on a 3D plane. Next, we multiply every feature point by a random transformation matrix to simulate the pose of the calibration pattern. Finally, we map the feature points on the pattern to catadioptric image plane by a set of viewing sphere parameters which is the ground truth.

For simulation data of Ying's method, the procedure is almost the same. We only have to generate a set of points in the same circle on a 3D plane, and map the circle point to catadioptric image plane by the same viewing sphere parameters.

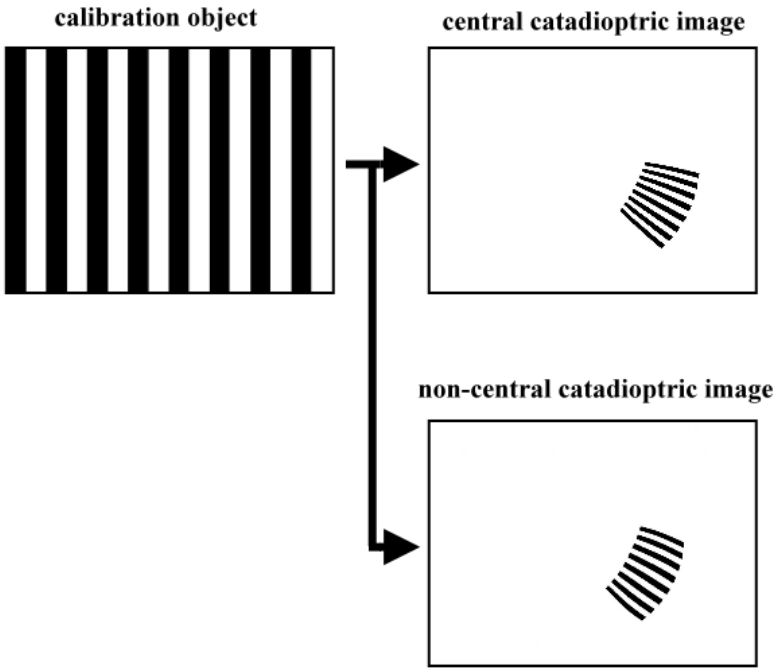

Figure A.2: **Simulation data generation for non-central catadioptric camera calibration.**

A.2 Simulation Data for Non-central Catadioptric Camera

We generate the simulation data of central and non-central catadioptric images by the reflected ray model (figure A.2). For simulation data of central catadioptric images, we set the lenses center of the perspective camera on another focus of hyperbolic mirror, and project a sets of feature points to the catadioptric image plane. For non-central catadioptric image, the distance between perspective camera and hyperbolic mirror is half of central one. As aforementioned in chapter 2, there is no close form solution for forward image formation of non-central catadioptric camera. Thus, we use an iterative method to generate the simulation data.

Appendix B

Central Catadioptric Camera Installation

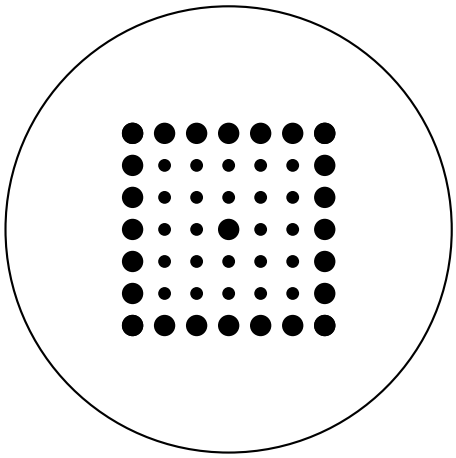

Figure B.1: **The calibration pattern we used in central catadioptric camera installation.** There are 49 (7×7) black feature points and a big black circle. Using the feature points, we can estimate the transformation matrix between the coordinate system of perspective camera and the pattern. According the transformation matrix, we can adjust the perspective camera until the we place it in the correct place. After that, we can place the mirror on the big black circle and then we accomplish the central catadioptric camera installation.

B.1 Central Catadioptric Camera Installation

It is important to place the perspective camera on the correct position, i.e. the lens center of perspective camera coincides with the another focus of hyperboloid to maintain the single viewpoint constraint. For this purpose, we use a planar calibration pattern to achieve this task (figure B.1). At first, we estimate the intrinsic parameters of the perspective camera using Zhang's method [50]. Then, we can adjust the relative position between the perspective camera and the mirror according to the extrinsic parameters until the relative position is precise enough.

In the perspective camera calibration, we estimate the intrinsic parameters of perspective camera using Zhang's method and the calibration pattern we used is shown in figure B.1 and is attached on a planar glass. In real experiment, we take images of planar

NO.	Focal length (mm)	Aspect ratio	Principal point	Reprojection error (pixel)
1	16.896	0.997	(551.498,396.174)	0.125
2	16.945	0.997	(547.116,394.412)	0.127
3	16.953	0.997	(549.408,393.328)	0.125
4	16.930	0.997	(548.442,396.614)	0.129
5	16.923	0.997	(547.748,393.819)	0.124

Table B.1: **Result of perspective camera calibration.** We experiments the procedure for five times and we choose the result with smallest reprojection error for our calibration result (result of NO. 5).

pattern for 12 times and extract the feature points by the following image processing techniques, image binarization, blob analysis and centroid estimation. After that, Using the feature points we estimated and their corresponding feature points on the planar pattern, the intrinsic parameters of perspective camera are calculated by function call of OpenCV library ($cvCalibrateCemera\_64d$) [30].

For verification of calibration result, we calculate the reprojection error of each feature point on the planar pattern. The reprojection error is the distance between the feature points we extract on the image plane and the points which are projected from the calibration pattern to the image plane by the camera parameters we estimated. We experiments the procedure for five times and choose the result with smallest reprojection error as our calibration result of the perspective camera (table B.1).

After the calibration of perspective camera, we setup the perspective camera and estimate the relative pose between the camera and the pattern by function call of OpenCV library ($cvFindExtrinsicCameraParams\_64d$). And the transformation matrix is a 3×4 matrix and it can be decomposed into four components, which including the pitch angle, roll angle, yaw angle and a translation vector, where the pitch, raw, and yaw angles describe the rotation about x axis, y axis and z axis and the translation vector is the distance between the lens center and the origin of calibration pattern. If the pitch and yaw angle is 0 degree and translation vector is the same with the specification of the hyperboloidal mirror, we put the hyperboloidal mirror on circle mark on planar pattern. Then, the perspective camera

	Pitch angle	Roll angle	Yaw angle	Translation vector (mm)
Goal	0.000	0.000	Not restricted	(0.000,0.000,409.300)
Our installation	-0.104	-0.065	0.226	(-0.075,0.026,409.545)

Table B.2: **Result of central catadioptric camera installation.** The first row is the gaol of installation, the pitch and roll angle is 0 degree and the yaw angle is not restricted. The goal of translation vector is calculated according to the specification of the mirror. The second row of the table is the result of our installation.

is located right on the focus of the hyperboloid. According to the result of transformation matrix, we can adjust the position of perspective camera until the installation is precise enough (table B.2).